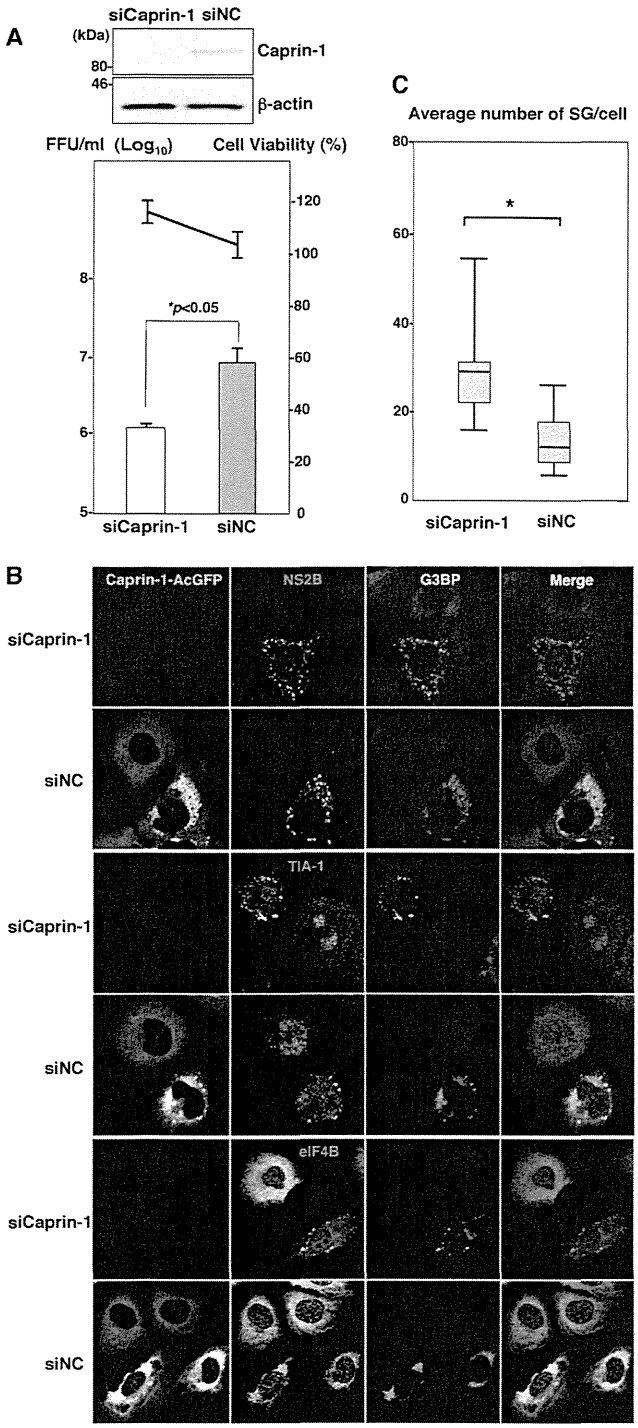

FIG 7 Knockdown of Caprin-1 cancels SG inhibition during JEV infection and suppresses viral propagation. (A) (Upper) The levels of expression of Caprin-1 in cells transfected with either siCaprin-1 or siNC was determined by immunoblotting using anti-Caprin-1 and anti-β-actin antibodies at 72 h posttransfection (top panel). At 48 h posttransfection with either siCaprin-1 or siNC, Huh7/Caprin-1-AcGFP cells were inoculated with JEV at an MOI of 0.5. At 24 h postinfection (72 h posttransfection), the infectious titers in the supernatants were determined by focus-forming assay in Vero cells (bottom panel, bar graph). Cell viability was determined at 72 h posttransfection and calculated as a percentage of the viability of cells treated with siNC (bottom panel, line graph). The results shown are from three independent assays, with the error bars representing the standard deviations. (B) At 48 h posttransfection with either siCaprin-1 or siNC, Huh7/Caprin-1-AcGFP cells were inoculated with JEV at an MOI of 0.5. The cellular localizations of SG-associated factors and JEV NS2B were determined at 24 h postinfection (72 h posttransfection) by immunofluorescence analysis with mouse anti-G3BP MAb and rabbit anti-NS2B PAb, rabbit anti-eIF4B PAb, or goat anti-TIA-1 PAb, followed by AF633-conjugated anti-mouse IgG and AF594-conjugated anti-rabbit IgG or AF594-conjugated anti-goat IgG, respectively. (C) Numbers of G3BP-positive foci in 30 cells prepared as described in panel B were counted. Lines, boxes, and error bars indicate the means, 25th to 75th percentiles, and 95th percentiles, respectively. The significance of differences between the means was determined by a Student's t test. *, $P < 0.01$.

tween JEV core protein and Caprin-1 was examined by a GST-pulldown assay using purified proteins expressed in bacteria. The His-tagged core protein was coprecipitated with GST-tagged Caprin-1, suggesting that JEV core protein directly interacts with Caprin-1 (Fig. 5F).

To further determine the cellular localization of Caprin-1 in JEV-infected cells, Caprin-1 fused with AcGFP (Caprin-1-AcGFP) was lentivirally expressed in Huh7 cells. The levels of expression and recruitment of Caprin-1-AcGFP into SGs were determined by immunoblotting and immunofluorescence analysis, respectively (Fig. 6A and B). In cells infected with JEV, Caprin-1-AcGFP was concentrated in the perinuclear region and colocalized with core protein and G3BP, while no colocalization of the proteins was observed in cells infected with DENV (Fig. 6C), suggesting that Caprin-1 directly interacts with JEV core protein in the perinuclear region of the infected cells.

Knockdown of Caprin-1 cancels SG inhibition during JEV infection and suppresses viral propagation. To assess the biological significance of the interaction of JEV core protein with Caprin-1 in JEV propagation, the expression of Caprin-1 was suppressed by using Caprin-1-specific siRNAs (siCaprin-1). Transfection of siCaprin-1 efficiently and specifically knocked down the expression of Caprin-1 with a slight increase of cell viability and decreased the production of infectious particles in the culture supernatants of cells infected with JEV, in comparison with those treated with a control siRNA (siNC) (Fig. 7A). Furthermore, immunofluorescence analyses revealed that knockdown of Caprin-1 increased the number of G3BP-positive granules colocalized with SG-associated factors, including TIA-1 and eIF4B, and inhibited the G3BP concentration in the perinuclear region (Fig. 7B and C). These results suggest that knockdown of Caprin-1 suppresses JEV propagation through the induction of SG formation.

Lys^{97} and Arg^{98} in the JEV core protein are crucial residues for the interaction with Caprin-1. To determine amino acid residues of the core protein that are required for the interaction with Caprin-1, we constructed a putative model based on the structural information of the DENV core protein previously resolved by nuclear magnetic resonance (NMR) (27), as shown in Fig. 8A. Based on this model, we selected hydrophobic amino acids, which were located on the solvent-exposed side in the α1 and α4 helices, as amino acid residues responsible for the binding to host proteins. Amino acid substitutions in each of the α-helices shown in Fig. 8B were designed in the context of FLAG-Core (Mα1 and Mα4), and the interaction of FLAG-Core mutants with Caprin-1 was examined by immunoprecipitation analysis. WT and Mα1, but not Mα4, core proteins were immunoprecipitated with Caprin-1 (Fig. 8B). To determine the amino acids responsible for interaction with Caprin-1, further alanine substitutions were introduced in the α4 helix, and the interaction was examined by immunopre-

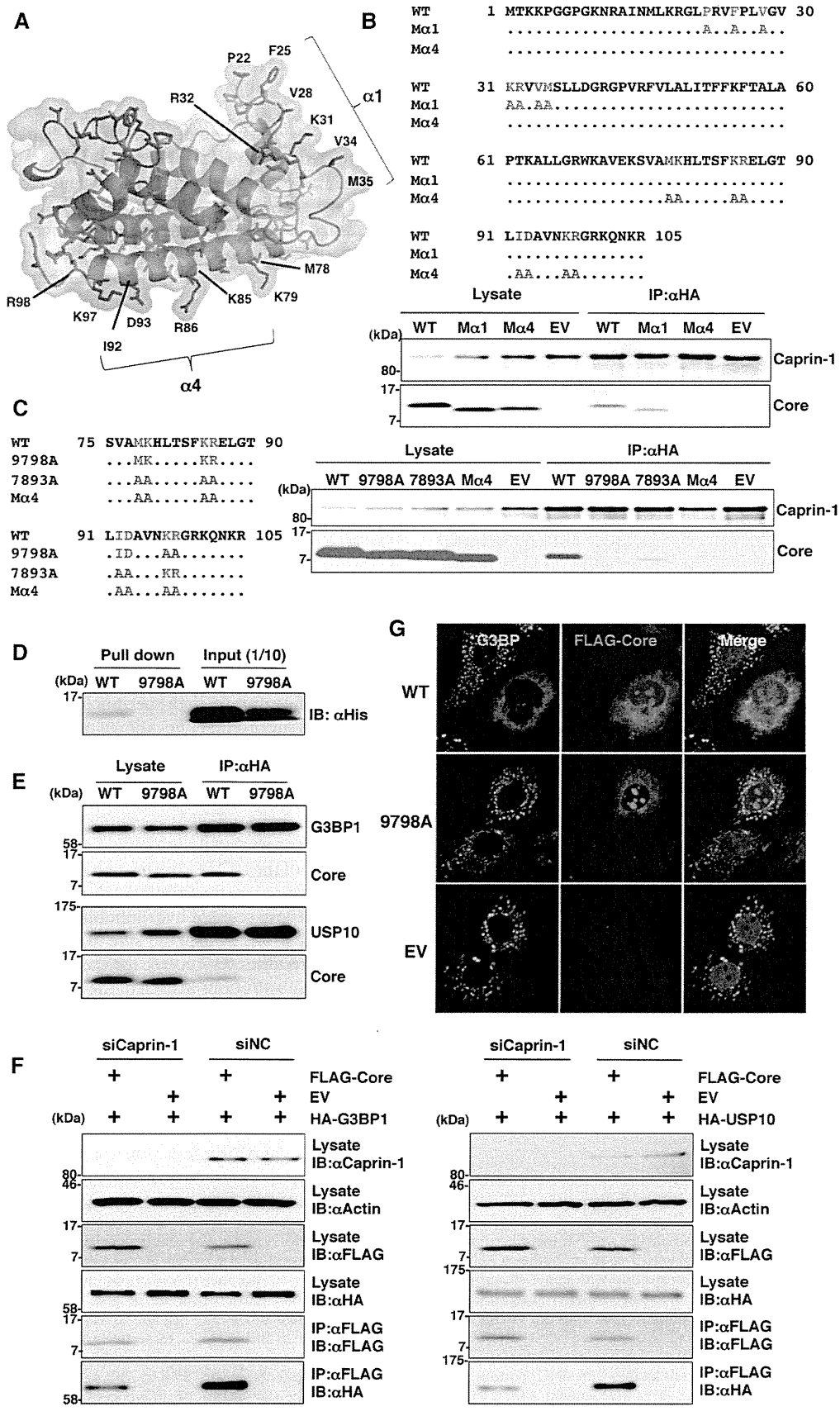

cipitation assay. As shown in Fig. 8C, double replacing both Lys^{97} and Arg^{98} with Ala (9798A) completely abrogated the interaction with Caprin-1. The importance of these two amino acids in the interaction with Caprin-1 was also confirmed by GST pulldown assay (Fig. 8D). These results indicate that Lys^{97} and Arg^{98} in the JEV core protein are crucial for the interaction with Caprin-1. Since G3BP has been reported to be one of the key molecules for SG formation and interacts with several SG component molecules including Caprin-1 and USP10 (28, 29), interactions of the core protein with SG components were examined by immunoprecipitation assay. The wild-type but not mutant 9798A core protein was associated with G3BP1 and USP10 (Fig. 8E). In addition, the knockdown of Caprin-1 weakened the interactions of core protein with G3BP1 or USP10 (Fig. 8F). These findings indicate that JEV core protein associates with several SG component molecules, such as G3BP1 and USP10, through the interaction with Caprin-1. Next, the role of the interaction between JEV core protein and Caprin-1 in the suppression of SG formation was examined by immunofluorescence analysis. Although the expression of the wild-type JEV core protein suppressed the SG formation induced by sodium arsenite treatment, as shown above, expression of the 9798A mutant did not (Fig. 8G), suggesting that the interaction of JEV core protein with Caprin-1 through Lys^{97} and Arg^{98} plays a crucial role in the inhibition of SG formation.

Interaction of the JEV core protein with Caprin-1 plays crucial roles not only in viral propagation *in vitro* but also in the pathogenesis in mice through the suppression of SG formation. To further examine the biological significance of the interaction between the JEV core protein and Caprin-1 in viral replication, we generated a mutant infectious cDNA clone (pMWJEAT/9798AA) of JEV encoding a mutant core protein deficient in the binding to Caprin-1 based on pMWJEAT. First, the cellular localization of the core protein in the 9798A mutant JEV-infected cells was examined by immunofluorescence analysis. The 9798A mutant core protein, as well as the wild-type core protein, was localized in the nucleus and the perinuclear region (Fig. 9A). However, the 9798A mutant core protein was not colocalized with Caprin-1, in contrast to the wild-type core protein. The sizes of infectious foci in Vero cells infected with the 9798A mutant were significantly smaller than those infected with the wild-type JEV (Fig. 9B). Furthermore, the infectious titers in C6/36 and Vero cells infected with the 9798A mutant were 6.1- and 12.6-fold lower than those infected with wild-type JEV at 48 h postinfection, respectively (Fig. 9C), suggesting that interaction of the JEV core protein with Caprin-1 plays crucial roles in the propagation of JEV in both insect and mammalian cells. Cells infected with the 9798A mutant induced SGs containing both G3BP and Caprin-1, in contrast to the accumulation of G3BP in the perinuclear region observed in those infected with the wild-type JEV (Fig. 9D). The numbers of foci in cells infected with the 9798A mutant were higher than those in cells infected with the wild-type JEV (Fig. 9E), indicating that the interaction of the JEV core protein with Caprin-1 is crucial for the suppression of SG formation. Finally, we examined the biological relevance of the interaction of JEV core protein with Caprin-1 in viral replication *in vivo*. Infectious particles were recovered from the cerebrums of ICR mice inoculated with wild-type JEV but not from those inoculated with the 9798A mutant (Fig. 9F). In addition, all 10 mice had died by 12 days postinoculation with the wild-type JEV, while only 1 mouse had died at day 10 postinoculation with the 9798A mutant (Fig. 9G). Collectively, these results suggest that the interaction of JEV core protein with Caprin-1 plays crucial roles not only in viral replication *in vitro* but also in pathogenesis in mice through the suppression of SG formation.

DISCUSSION

Viruses are obligatory intracellular parasites, and their life cycles rely on host cellular functions. Many viruses have evolved to inhibit SG formation and thereby evade the host translation shutoff mechanism and facilitate viral replication (6, 30), while some viruses co-opt molecules regulating SG formation for viral replication (11, 31). The vaccinia virus subverts SG components to generate aggregates containing G3BP, Caprin-1, eIF4G, eIF4E, and mRNA of the virus, but not of the host, in order to stimulate viral translation (11). Replication, translation, and assembly of transmissible gastroenteritis coronavirus, a member of the *Coronaviridae* family, are regulated by the interaction of polypyrimidine tract-binding protein and TIA-1 with viral RNA (31). HIV-1 utilizes Staufen1, which is a principal component of SG, in the viral RNA selection to form ribonucleoproteins (RNPs) through interaction with Gag protein, instead of SG translation silencing (8). In the case of flaviviruses, TIA-1 and TIAR bind to the 3′ untranslated region (UTR) of the negative-stranded RNA of WNV to facilitate viral replication (16), and G3BP1, Caprin-1, and USP10 interact with DENV RNA, although the biological significance of these interactions remains unknown (26). In this study, we have shown that JEV infection suppresses SG formation by the recruitment of several effector molecules promoting SG assembly, including G3BP and USP10, to the perinuclear region through the interaction of JEV core protein with Caprin-1. Furthermore, a mutant JEV carrying a core protein incapable of binding to

FIG 8 Lys^{97} and Arg^{98} in the JEV core protein are crucial residues for the interaction with Caprin-1. (A) Putative structural model of the core protein homodimer of JEV deduced from that of DENV obtained from the Protein Data Bank (accession number 1R6R) by using PyMOL software. The two α helices (α1 and α4) are indicated. (B) FLAG-Core mutants in which the hydrophobic amino acid residues in the α1 helix (Mα1) or α4 helix (Mα4) were replaced with alanine were coexpressed with HA-Caprin-1 in 293T cells, immunoprecipitated (IP) with anti-HA antibody, and examined by immunoblotting (IB) with anti-HA or anti-FLAG antibody. (C) FLAG-Core mutants in which the Met^{78}, Lys^{79}, Lys^{85}, Arg^{86}, Ile^{92}, and Asp^{93} (7893A) or Lys^{97} and Arg^{98} (9798A) in the α4 helix domain were replaced with alanine were coexpressed with HA-Caprin-1 in 293T cells and examined as described in panel B. (D) The His-tagged JEV core protein (WT or 9798A) was incubated with GST-fused Caprin-1 for 2 h at 4°C, and the precipitates obtained by GST pulldown assay were subjected to immunoblotting with anti-His antibody. (E) FLAG-Core (WT or 9798A) was coexpressed with HA-G3BP1 or HA-USP10 in 293T cells, immunoprecipitated with anti-HA antibody, and immunoblotted with anti-HA and anti-FLAG antibodies. (F) FLAG-JEV Core was coexpressed with HA-G3BP1 or HA-USP10 in 293T cells transfected with either siCaprin-1 or siNC at 72 h posttransfection, immunoprecipitated with anti-FLAG antibody, and immunoblotted with anti-HA and anti-FLAG antibodies. The cell lysates were also subjected to immunoblotting with anti-Caprin-1 and anti-β-actin antibodies to evaluate the knockdown efficiency of Caprin-1. (G) The cellular localizations of G3BP and FLAG-Core (WT or 9798A) were determined at 24 h posttransfection after treatment with 1.0 mM sodium arsenite for 30 min at 37°C by immunofluorescence analysis with mouse anti-G3BP MAb and rabbit anti-FLAG PAb, followed by AF488-conjugated anti-mouse IgG and AF594-conjugated anti-rabbit IgG, respectively. Cell nuclei were stained with DAPI (blue).

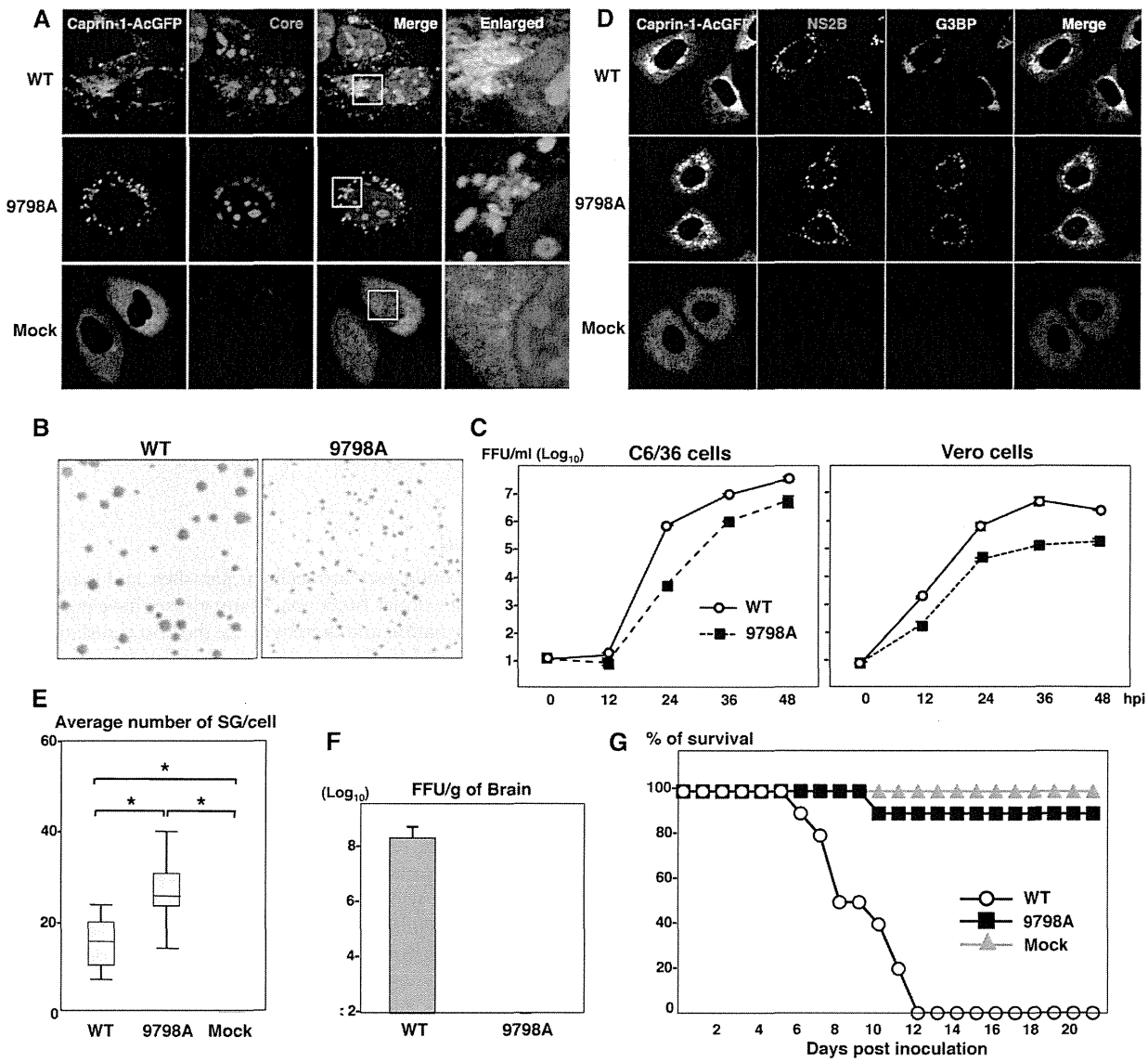

FIG 9 Interaction of JEV core protein with Caprin-1 plays crucial roles not only in viral replication *in vitro* but also in pathogenesis in mice through the suppression of SG formation. (A) Huh7/Caprin-1-AcGFP cells were infected with JEV (WT or 9798A mutant) at an MOI of 1.0, and the cellular localizations of Caprin-1-AcGFP and JEV core protein were determined at 24 h postinfection by immunofluorescence analysis with rabbit anti-core PAb and AF594-conjugated anti-rabbit IgG. Cell nuclei were stained with DAPI (blue). (B) Focus formation of JEV (WT or 9798A mutant) in Vero cells incubated in methylcellulose overlay medium at 48 h postinfection. The infectious foci were immunostained as described previously (20). (C) Growth kinetics of JEV (WT or 9798A mutant) in C6/36 and Vero cells infected at an MOI of 0.1. Infectious titers in the culture supernatants harvested at the indicated times were determined by focus-forming assays in Vero cells. Means of three experiments are indicated. (D) Huh7/Caprin-1-AcGFP cells were infected with either WT or 9798A at an MOI of 0.5, and cellular localizations of Caprin-1-AcGFP, G3BP (blue), and JEV NS2B (red) were determined at 24 h postinfection by immunofluorescence analysis with mouse anti-G3BP MAb and rabbit anti-NS2B PAb, followed by AF633-conjugated anti-mouse IgG and AF594-conjugated anti-rabbit IgG, respectively. (E) Numbers >of G3BP-positive foci in 30 cells prepared as described in panel D were counted. Lines, boxes, and error bars indicate the means, 25th to 75th percentiles, and 95th percentiles, respectively. The significance of differences between the means was determined by Student's *t* test. *, $P < 0.01$. (F) Infectious titers in the cerebrums of mice at 7 days postintraperitoneal inoculation with 5×10^4 FFU/100 μl of either WT or 9798A virus were determined in Vero cells. The means of titers in the homogenates of the cerebrums from three mice are indicated. The detection limit is 10^2 FFU/g of cerebrum. (G) Percentages of surviving mice ($n = 10$) after intraperitoneal inoculation with 5×10^4 FFU of either WT or 9798A virus. Mock, inoculation with DMEM.

Caprin-1 exhibited reduced replication *in vitro* and attenuated pathogenicity in mice.

G3BP is one of the key molecules involved in the SG aggregation process and self-oligomerizes in a phosphorylation-dependent manner to sequester mRNA in SGs (4). Therefore, G3BP knocked down cells (6) and G3BP knockout mouse embryonic fibroblast cells are deficient in the SG formation. In addition, G3BP sequestration inhibits SG formation in response to arsenite treatment (32). Caprin-1, known as RNA granule protein 105 or p137 (33), also participates in SG formation through phosphorylation of eIF2α (28) and is ubiquitously expressed in the cytoplasm. Caprin-1 regulates the transport and translation of mRNAs

of proteins involved in the synaptic plasticity in neurons (34) and cellular proliferation and migration in multiple cell types (28) through an interaction with G3BP. USP10, another SG-associated molecule, also interacts with G3BP and forms the G3BP/USP10 complex (29), suggesting that several SG-associated RBPs participate in the formation of a protein-protein network. In this study, the JEV core protein was shown to directly interact with Caprin-1, to sequester several key molecule complexes involved in SG formation to the perinuclear region in cells infected with JEV, and to facilitate viral propagation through the suppression of SG formation.

Flaviviruses replicate at a relatively low rate in comparison with most of the other positive-stranded RNA viruses, and thus rapid shutdown of host cellular protein synthesis would be deleterious for the viral life cycle. In cells infected with JEV, several SG components were colocalized with the core protein in the perinuclear region, while in those infected with WNV or DENV, SG components were accumulated in a replication complex composed of viral RNA and nonstructural proteins. In addition, the phosphorylation of eIF2α induced by arsenite was completely canceled by the infection with WNV or DENV, whereas the suppression of the phosphorylation was limited in JEV infection (15). Incorporation of the nascent viral RNA into the membranous structure induced by viral nonstructural proteins prevents PKR activation and inhibits SG formation in cells infected with WNV (17). In cells infected with hepatitis C virus (HCV), which belongs to the genus *Hepacivirus* in the family *Flaviviridae*, induction of SG formation was observed in the early stage of infection, in contrast to the inhibition of the arsenite-induced SG formation in the late stage (35). Several SG components, such as G3BP1, PABP1, and ataxin-2, were colocalized with HCV core protein around lipid droplets (35), and G3BP1 was also associated with the NS5B protein and the 5′ terminus of the minus-strand viral RNA (36) to mediate efficient viral replication. Collectively, these data suggest that flaviviruses have evolved to regulate cellular processes involved in SG formation through various strategies.

PKR is one of the interferon-stimulated genes and plays a crucial role in antiviral defense through phosphorylation of eIF2α, which leads to host translational shutoff (37, 38). In the early stage of flavivirus infection, both positive- and negative-stranded RNAs transcribe at low levels, while genomic RNA predominantly synthesizes in the late stage of infection (39). It was shown that activation of PKR was suppressed (40) or only induced in the late stage of WNV infection (41) and impaired by the expression of HCV NS5A (42–44). Very recently, JEV NS2A was shown to suppress PKR activation through inhibition of dimerization of PKR in the early stage but not in the late stage of infection (45). In this study, we have shown that JEV core protein interacts with Caprin-1 and inhibits SG formation downstream of the phosphorylation of eIF2α in the late stage of infection, suggesting that JEV has evolved to escape from host antiviral responses in the multiple stages of viral replication by using structural and nonstructural proteins.

The flavivirus core protein is a multifunctional protein involved in many aspects of the viral life cycle. In addition to the formation of viral nucleocapsid through the interaction with viral RNA (as a structural protein) (46), flavivirus core proteins interact with various host factors, such as B23 (47), Jab1 (48), hnRNP K (49), and hnRNP A2 (23), and regulate viral replication and/or modify the host cell environment (as a nonstructural protein). Although further investigations are needed to clarify the precise mechanisms underlying the circumvention of SG formation through the interaction of JEV core protein with Caprin-1, leading to efficient propagation *in vitro* and pathogenicity in mice, these findings could help not only to provide new insight into strategies by which viruses escape host stress responses but also to develop novel antiviral agents for flavivirus infection.

ACKNOWLEDGMENTS

We thank M. Tomiyama for secretarial assistance. We also thank K. Saito and T. Wakita for technical advice and the infectious clone of JEV, respectively.

This work was supported in part by grants-in-aid from the Ministry of Health, Labor, and Welfare, the Ministry of Education, Culture, Sports, Science, and Technology, and the Osaka University Global Center of Excellence Program. H. Katoh is a research fellow of the Japanese Society for the Promotion of Science.

REFERENCES

1. **Nover L, Scharf KD, Neumann D.** 1989. Cytoplasmic heat shock granules are formed from precursor particles and are associated with a specific set of mRNAs. Mol. Cell. Biol. **9**:1298–1308.
2. **Anderson P, Kedersha N.** 2002. Stressful initiations. J. Cell Sci. **115**:3227–3234.
3. **Gilks N, Kedersha N, Ayodele M, Shen L, Stoecklin G, Dember LM, Anderson P.** 2004. Stress granule assembly is mediated by prion-like aggregation of TIA-1. Mol. Biol. Cell **15**:5383–5398.
4. **Tourriere H, Chebli K, Zekri L, Courselaud B, Blanchard JM, Bertrand E, Tazi J.** 2003. The RasGAP-associated endoribonuclease G3BP assembles stress granules. J. Cell Biol. **160**:823–831.
5. **Kedersha N, Cho MR, Li W, Yacono PW, Chen S, Gilks N, Golan DE, Anderson P.** 2000. Dynamic shuttling of TIA-1 accompanies the recruitment of mRNA to mammalian stress granules. J. Cell Biol. **151**:1257–1268.
6. **White JP, Cardenas AM, Marissen WE, Lloyd RE.** 2007. Inhibition of cytoplasmic mRNA stress granule formation by a viral proteinase. Cell Host Microbe **2**:295–305.
7. **Khaperskyy DA, Hatchette TF, McCormick C.** 2012. Influenza A virus inhibits cytoplasmic stress granule formation. FASEB J. **26**:1629–1639.
8. **Abrahamyan LG, Chatel-Chaix L, Ajamian L, Milev MP, Monette A, Clement JF, Song R, Lehmann M, DesGroseillers L, Laughrea M, Boccaccio G, Mouland AJ.** 2010. Novel Staufen1 ribonucleoproteins prevent formation of stress granules but favour encapsidation of HIV-1 genomic RNA. J. Cell Sci. **123**:369–383.
9. **McInerney GM, Kedersha NL, Kaufman RJ, Anderson P, Liljestrom P.** 2005. Importance of eIF2α phosphorylation and stress granule assembly in alphavirus translation regulation. Mol. Biol. Cell **16**:3753–3763.
10. **Smith JA, Schmechel SC, Raghavan A, Abelson M, Reilly C, Katze MG, Kaufman RJ, Bohjanen PR, Schiff LA.** 2006. Reovirus induces and benefits from an integrated cellular stress response. J. Virol. **80**:2019–2033.
11. **Katsafanas GC, Moss B.** 2007. Colocalization of transcription and translation within cytoplasmic poxvirus factories coordinates viral expression and subjugates host functions. Cell Host Microbe **2**:221–228.
12. **Misra UK, Kalita J.** 2010. Overview: Japanese encephalitis. Prog. Neurobiol. **91**:108–120.
13. **Sumiyoshi H, Mori C, Fuke I, Morita K, Kuhara S, Kondou J, Kikuchi Y, Nagamatu H, Igarashi A.** 1987. Complete nucleotide sequence of the Japanese encephalitis virus genome RNA. Virology **161**:497–510.
14. **Murray CL, Jones CT, Rice CM.** 2008. Architects of assembly: roles of *Flaviviridae* non-structural proteins in virion morphogenesis. Nat. Rev. Microbiol. **6**:699–708.
15. **Emara MM, Brinton MA.** 2007. Interaction of TIA-1/TIAR with West Nile and dengue virus products in infected cells interferes with stress granule formation and processing body assembly. Proc. Natl. Acad. Sci. U. S. A. **104**:9041–9046.
16. **Li W, Li Y, Kedersha N, Anderson P, Emara M, Swiderek KM, Moreno GT, Brinton MA.** 2002. Cell proteins TIA-1 and TIAR interact with the 3′ stem-loop of the West Nile virus complementary minus-strand RNA and facilitate virus replication. J. Virol. **76**:11989–12000.
17. **Courtney SC, Scherbik SV, Stockman BM, Brinton MA.** 2012. West Nile

virus infections suppress early viral RNA synthesis and avoid inducing the cell stress granule response. J. Virol. 86:3647–3657.
18. Kambara H, Tani H, Mori Y, Abe T, Katoh H, Fukuhara T, Taguwa S, Moriishi K, Matsuura Y. 2011. Involvement of cyclophilin B in the replication of Japanese encephalitis virus. Virology 412:211–219.
19. Mori Y, Yamashita T, Tanaka Y, Tsuda Y, Abe T, Moriishi K, Matsuura Y. 2007. Processing of capsid protein by cathepsin L plays a crucial role in replication of Japanese encephalitis virus in neural and macrophage cells. J. Virol. 81:8477–8487.
20. Mori Y, Okabayashi T, Yamashita T, Zhao Z, Wakita T, Yasui K, Hasebe F, Tadano M, Konishi E, Moriishi K, Matsuura Y. 2005. Nuclear localization of Japanese encephalitis virus core protein enhances viral replication. J. Virol. 79:3448–3458.
21. Kambara H, Fukuhara T, Shiokawa M, Ono C, Ohara Y, Kamitani W, Matsuura Y. 2012. Establishment of a novel permissive cell line for the propagation of hepatitis C virus by expression of microRNA miR122. J. Virol. 86:1382–1393.
22. Zhao Z, Date T, Li Y, Kato T, Miyamoto M, Yasui K, Wakita T. 2005. Characterization of the E-138 (Glu/Lys) mutation in Japanese encephalitis virus by using a stable, full-length, infectious cDNA clone. J. Gen. Virol. 86:2209–2220.
23. Katoh H, Mori Y, Kambara H, Abe T, Fukuhara T, Morita E, Moriishi K, Kamitani W, Matsuura Y. 2011. Heterogeneous nuclear ribonucleoprotein A2 participates in the replication of Japanese encephalitis virus through an interaction with viral proteins and RNA. J. Virol. 85:10976–10988.
24. Hamamoto I, Nishimura Y, Okamoto T, Aizaki H, Liu M, Mori Y, Abe T, Suzuki T, Lai MM, Miyamura T, Moriishi K, Matsuura Y. 2005. Human VAP-B is involved in hepatitis C virus replication through interaction with NS5A and NS5B. J. Virol. 79:13473–13482.
25. Jones CT, Ma L, Burgner JW, Groesch TD, Post CB, Kuhn RJ. 2003. Flavivirus capsid is a dimeric alpha-helical protein. J. Virol. 77:7143–7149.
26. Ward AM, Bidet K, Yinglin A, Ler SG, Hogue K, Blackstock W, Gunaratne J, Garcia-Blanco MA. 2011. Quantitative mass spectrometry of DENV-2 RNA-interacting proteins reveals that the DEAD-box RNA helicase DDX6 binds the DB1 and DB2 3′ UTR structures. RNA Biol. 8:1173–1186.
27. Ma L, Jones CT, Groesch TD, Kuhn RJ, Post CB. 2004. Solution structure of dengue virus capsid protein reveals another fold. Proc. Natl. Acad. Sci. U. S. A. 101:3414–3419.
28. Solomon S, Xu Y, Wang B, David MD, Schubert P, Kennedy D, Schrader JW. 2007. Distinct structural features of Caprin-1 mediate its interaction with G3BP-1 and its induction of phosphorylation of eukaryotic translation initiation factor 2α, entry to cytoplasmic stress granules, and selective interaction with a subset of mRNAs. Mol. Cell. Biol. 27: 2324–2342.
29. Soncini C, Berdo I, Draetta G. 2001. Ras-GAP SH3 domain binding protein (G3BP) is a modulator of USP10, a novel human ubiquitin specific protease. Oncogene 20:3869–3879.
30. Montero H, Rojas M, Arias CF, Lopez S. 2008. Rotavirus infection induces the phosphorylation of eIF2α but prevents the formation of stress granules. J. Virol. 82:1496–1504.
31. Sola I, Galan C, Mateos-Gomez PA, Palacio L, Zuniga S, Cruz JL, Almazan F, Enjuanes L. 2011. The polypyrimidine tract-binding protein affects coronavirus RNA accumulation levels and relocalizes viral RNAs to novel cytoplasmic domains different from replication-transcription sites. J. Virol. 85:5136–5149.
32. Hinton SD, Myers MP, Roggero VR, Allison LA, Tonks NK. 2010. The pseudophosphatase MK-STYX interacts with G3BP and decreases stress granule formation. Biochem. J. 427:349–357.
33. Grill B, Wilson GM, Zhang KX, Wang B, Doyonnas R, Quadroni M, Schrader JW. 2004. Activation/division of lymphocytes results in increased levels of cytoplasmic activation/proliferation-associated protein-1: prototype of a new family of proteins. J. Immunol. 172:2389–2400.
34. Shiina N, Shinkura K, Tokunaga M. 2005. A novel RNA-binding protein in neuronal RNA granules: regulatory machinery for local translation. J. Neurosci. 25:4420–4434.
35. Ariumi Y, Kuroki M, Kushima Y, Osugi K, Hijikata M, Maki M, Ikeda M, Kato N. 2011. Hepatitis C virus hijacks P-body and stress granule components around lipid droplets. J. Virol. 85:6882–6892.
36. Yi Z, Pan T, Wu X, Song W, Wang S, Xu Y, Rice CM, Macdonald MR, Yuan Z. 2011. Hepatitis C virus co-opts Ras-GTPase-activating protein-binding protein 1 for its genome replication. J. Virol. 85:6996–7004.
37. Gale M, Jr, Katze MG. 1998. Molecular mechanisms of interferon resistance mediated by viral-directed inhibition of PKR, the interferon-induced protein kinase. Pharmacol. Ther. 78:29–46.
38. Pindel A, Sadler A. 2011. The role of protein kinase R in the interferon response. J. Interferon Cytokine Res. 31:59–70.
39. Chu PW, Westaway EG. 1985. Replication strategy of Kunjin virus: evidence for recycling role of replicative form RNA as template in semiconservative and asymmetric replication. Virology 140:68–79.
40. Elbahesh H, Scherbik SV, Brinton MA. 2011. West Nile virus infection does not induce PKR activation in rodent cells. Virology 421:51–60.
41. Samuel MA, Whitby K, Keller BC, Marri A, Barchet W, Williams BR, Silverman RH, Gale M, Jr, Diamond MS. 2006. PKR and RNase L contribute to protection against lethal West Nile Virus infection by controlling early viral spread in the periphery and replication in neurons. J. Virol. 80:7009–7019.
42. Gale M, Jr, Blakely CM, Kwieciszewski B, Tan SL, Dossett M, Tang NM, Korth MJ, Polyak SJ, Gretch DR, Katze MG. 1998. Control of PKR protein kinase by hepatitis C virus nonstructural 5A protein: molecular mechanisms of kinase regulation. Mol. Cell. Biol. 18:5208–5218.
43. Gale MJ, Jr, Korth MJ, Tang NM, Tan SL, Hopkins DA, Dever TE, Polyak SJ, Gretch DR, Katze MG. 1997. Evidence that hepatitis C virus resistance to interferon is mediated through repression of the PKR protein kinase by the nonstructural 5A protein. Virology 230:217–227.
44. He Y, Tan SL, Tareen SU, Vijaysri S, Langland JO, Jacobs BL, Katze MG. 2001. Regulation of mRNA translation and cellular signaling by hepatitis C virus nonstructural protein NS5A. J. Virol. 75:5090–5098.
45. Tu YC, Yu CY, Liang JJ, Lin E, Liao CL, Lin YL. 2012. Blocking dsRNA-activated protein kinase PKR by Japanese encephalitis virus nonstructural protein 2A. J. Virol. 86:10347–10358.
46. Khromykh AA, Westaway EG. 1996. RNA binding properties of core protein of the flavivirus Kunjin. Arch. Virol. 141:685–699.
47. Tsuda Y, Mori Y, Abe T, Yamashita T, Okamoto T, Ichimura T, Moriishi K, Matsuura Y. 2006. Nucleolar protein B23 interacts with Japanese encephalitis virus core protein and participates in viral replication. Microbiol. Immunol. 50:225–234.
48. Oh W, Yang MR, Lee EW, Park KM, Pyo S, Yang JS, Lee HW, Song J. 2006. Jab1 mediates cytoplasmic localization and degradation of West Nile virus capsid protein. J. Biol. Chem. 281:30166–30174.
49. Chang CJ, Luh HW, Wang SH, Lin HJ, Lee SC, Hu ST. 2001. The heterogeneous nuclear ribonucleoprotein K (hnRNP K) interacts with dengue virus core protein. DNA Cell Biol. 20:569–577.

JVI
Journals.ASM.org

Expression of MicroRNA miR-122 Facilitates an Efficient Replication in Nonhepatic Cells upon Infection with Hepatitis C Virus

Takasuke Fukuhara,[a] Hiroto Kambara,[a] Mai Shiokawa,[a] Chikako Ono,[a] Hiroshi Katoh,[a] Eiji Morita,[a] Daisuke Okuzaki,[b] Yoshihiko Maehara,[c] Kazuhiko Koike,[d] and Yoshiharu Matsuura[a]

Department of Molecular Virology[a] and DNA-Chip Developmental Center for Infectious Diseases,[b] Research Institute for Microbial Diseases, Osaka University, Osaka, Japan; Department of Surgery and Science, Graduate School of Medical Sciences, Kyushu University, Fukuoka, Japan[c]; and Department of Gastroenterology, Graduate School of Medicine, University of Tokyo, Tokyo, Japan[d]

Hepatitis C virus (HCV) is one of the most common etiologic agents of chronic liver diseases, including liver cirrhosis and hepatocellular carcinoma. In addition, HCV infection is often associated with extrahepatic manifestations (EHM), including mixed cryoglobulinemia and non-Hodgkin's lymphoma. However, the mechanisms of cell tropism of HCV and HCV-induced EHM remain elusive, because *in vitro* propagation of HCV has been limited in the combination of cell culture-adapted HCV (HCVcc) and several hepatic cell lines. Recently, a liver-specific microRNA called miR-122 was shown to facilitate the efficient propagation of HCVcc in several hepatic cell lines. In this study, we evaluated the importance of miR-122 on the replication of HCV in nonhepatic cells. Among the nonhepatic cell lines expressing functional HCV entry receptors, Hec1B cells derived from human uterus exhibited a low level of replication of the HCV genome upon infection with HCVcc. Exogenous expression of miR-122 in several cells facilitates efficient viral replication but not production of infectious particles, probably due to the lack of hepatocytic lipid metabolism. Furthermore, expression of mutant miR-122 carrying a substitution in a seed domain was required for efficient replication of mutant HCVcc carrying complementary substitutions in miR-122-binding sites, suggesting that specific interaction between miR-122 and HCV RNA is essential for the enhancement of viral replication. In conclusion, although miR-122 facilitates efficient viral replication in nonhepatic cells, factors other than miR-122, which are most likely specific to hepatocytes, are required for HCV assembly.

More than 170 million individuals worldwide are infected with hepatitis C virus (HCV), and cirrhosis and hepatocellular carcinoma induced by HCV infection are life-threatening diseases (57). Although therapy combining pegylated interferon (IFN) and ribavirin has achieved a sustained virological response in 50% of individuals infected with HCV genotype 1 (37), a more effective therapeutic modality for HCV infection is needed (46). The establishment of *in vivo* and *in vitro* infection systems has been hampered by the narrow host range and tissue tropism of HCV. Although the chimpanzee is the only experimental animal susceptible to HCV infection, it is difficult to use the chimpanzee in experiments due to ethical concerns (3). Furthermore, robust *in vitro* HCV propagation is limited to the combination of cell culture-adapted clones based on the genotype 2a JFH1 strain (HCVcc) and human hepatoma cell lines, including Huh7, Hep3B, and HepG2 (29, 43, 62).

It is well-known that HCV mainly infects hepatocytes. However, the precise mechanism underlying the liver tropism of HCV has not been clarified. Chronic hepatitis C virus infection is often associated with at least one extrahepatic manifestation (EHM), including mixed cryoglobulinemia, non-Hodgkin's lymphoma, lichen planus, thyroiditis, diabetes mellitus, Sjögren syndrome, and arthritis (19). EHMs are frequently more serious than hepatic disease in some patients and sometimes occur even in patients with persistently normal liver functions (19). Mixed cryoglobulinemia is the most-well-characterized HCV-associated disease and is curable by viral clearance through antiviral therapies (6). Although replication of HCV RNA in peripheral blood mononuclear cells (PBMCs) and neuronal cells at a low level was suggested (64), the biological significance of the extrahepatic replication of HCV, particularly in the development of EHMs, is not well understood.

MicroRNAs (miRNAs) are small noncoding RNAs consisting of 20 to 25 nucleotides that modulate gene expression in plants and animals (1, 24). Most miRNAs negatively regulate translation through the interaction with the 3′ untranslated region (UTR) of mRNA in a sequence-specific manner. miRNA 122 (miR-122) is liver specific, is the most abundantly expressed miRNA in the liver, and represses the translation of several mRNAs (5, 7). Jopling et al. reported for the first time that the inhibition of miR-122 dramatically decreased RNA replication in HCV subgenomic replicon (SGR) cells (28). In addition, several reports revealed that a specific interaction between the seed domain of miR-122 and the complementary sequences in the 5′ UTR of HCV RNA is essential for the enhancement of translation and replication of the HCV genome (21, 25, 27, 36). Endogenous expression levels of miR-122 are significantly higher in Huh7 cells than in other hepatic and nonhepatic cell lines (Fig. 1). In addition, previous reports showed that miR-122 expression enhanced the replication of SGR RNA in human embryonic kidney 293 (HEK293) cells and mouse embryonic fibroblasts (MEFs) (8, 35). Furthermore, it was recently shown that exogenous expression of miR-122 facilitates the efficient propagation of HCVcc in Hep3B and HepG2 cells, which are

Received 4 March 2012 Accepted 10 May 2012
Published ahead of print 16 May 2012
Address correspondence to Yoshiharu Matsuura, matsuura@biken.osaka-u.ac.jp.

doi:10.1128/JVI.00567-12

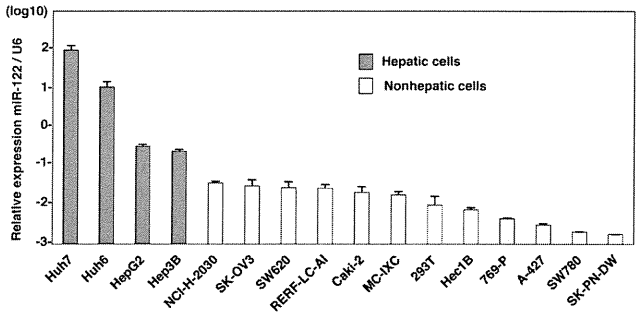

FIG 1 Endogenous expression levels of miR-122 in hepatic and nonhepatic cells. Total miRNAs were extracted from Huh7, Huh6, HepG2, Hep3B, NCI-H-2030, SK-OV3, SW620, RERF-LC-AI, Caki-2, MC-IXC, 293T, Hec1B, 769-P, A-427, SW780, and SK-PN-DW cells, and the expression levels of miR-122 were determined by qRT-PCR.

nonpermissive for HCVcc propagation (29, 43). These results suggest that the high susceptibility of Huh7 cells to the propagation of HCVcc is attributable to the high expression level of miR-122 and raise the possibility of expanding the HCV host range through the exogenous expression of miR-122 in nonhepatic cells.

In this study, we assessed the effect of miR-122 expression on the replication of HCVcc and SGR RNA in several nonhepatic cell lines. Although the exogenous expression of miR-122 in the cell lines facilitates significant RNA replication through a gene-specific interaction between miR-122 and 5′ UTR of HCV RNA, no infectivity was detected in either the cells or the culture supernatants. The current study suggests that the expression of miR-122 plays an important role in HCV cell tropism, as well as in the possible involvement of nonhepatic cells in EHM, through an incomplete propagation of HCV.

MATERIALS AND METHODS

NextBio Body Atlas. The NextBio Body Atlas application presents an aggregated analysis of gene expression across various normal tissues, normal cell types, and cancer cell lines. It enables us to investigate the expression of individual genes as well as gene sets. Samples for Body Atlas data are obtained from publicly available studies that are internally curated, annotated, and processed (31). Body Atlas measurements are generated from all available RNA expression studies that used Affymetrix U133 Plus or U133A Genechip arrays for human studies. The results corresponding to 128 human tissue samples were incorporated from 1,067 arrays, the results corresponding to 157 human cell types were incorporated from 1,474 arrays, and the results corresponding to 359 human cancer cell lines were incorporated from 376 arrays. Gene queries return a list of relevant tissues or cell types rank ordered by absolute gene expression and grouped by body systems or across all body systems. In the current analysis, we screened for nonhepatic cell lines expressing HCV receptor candidates, including CD81, SR-BI, claudin1 (CLDN1), and occludin (OCLN), or very-low-density lipoprotein (VLDL)-associated proteins, including apolipoprotein E (ApoE), ApoB, and microsomal triglyceride transfer protein (MTTP). A detailed analysis protocol developed by NextBio was described previously (31). The raw data used in this application are derived from the GSK Cancer Cell Line data deposited at the National Cancer Institute website (https://array.nci.nih.gov/caarray/project/woost-00041) and additionally from NCBI Gene Expression Omnibus (GEO) accession number GSE5720 for cell lines SK-OV-3 and SW620.

Sample collection and RNA extraction for microarray analysis. Total RNAs extracted from cells were purified by using an miRNeasy kit (Qiagen, Valencia, CA) according to the manufacturer's protocol. Eluted RNAs were quantified using a Nanodrop ND-1000 (version 3.5.2) spectrophotometer (Thermo Scientific, Wartham, MA). RNA integrity was evaluated using the RNA 6000 LabChip kit and bioanalyzer (Agilent Technologies, Santa Clara, CA). Each RNA that had an RNA integrity number (RIN) greater than 9.0 was used for the microarray experiments.

Microarray experiment. Expression profiling was generated using the 4 × 44K whole-human-genome oligonucleotide microarray (version 2.0) G4845A (Agilent Technologies). Each microarray uses 44,495 probes to interrogate 27,958 Entrez gene RNAs. One hundred nanograms of total RNA was reverse transcribed into double-stranded cDNAs by AffinityScript multiple-temperature reverse transcriptase and amplified for 2 h at 40°C. The resulting cDNAs were subsequently used for *in vitro* transcription by the T7 polymerase and labeled with cyanine-3-labeled cytosine triphosphate (Perkin Elmer, Waltham, MA) for 2 h at 40°C using a low-input Quick-Amp labeling kit (Agilent Technologies) according to the manufacturer's protocol. After labeling, the rates of dye incorporation and quantification were measured with a Nanodrop ND-1000 (version 3.5.2) spectrophotometer (Thermo Scientific), and then the cRNAs were fragmented for 30 min at 60°C in the dark. Differentially labeled samples of 1,650 ng of cRNA were hybridized on Agilent 4 × 44K whole-genome arrays (version 2.0; 026652; Agilent Design) at 65°C for 17 h with rotation in the dark. Hybridization was performed using a gene expression hybridization kit (Agilent Technologies) following the manufacturer's instructions. After washing in gene expression washing buffer, each slide was scanned with the Agilent microarray scanner G2505C. Feature extraction software (version 10.5.1.1) employing defaults for all parameters was used to convert the images into gene expression data. Raw data were imported into a Subio platform (version 1.12) for database management and quality control. Raw intensity data were normalized against GAPDH (glyceraldehyde-3-phosphate dehydrogenase) expression levels for further analysis. These raw data have been accepted by GEO (a public repository for microarray data aimed at storing minimum information about microarray experiments [MIAME]).

Plasmids. The cDNA clones of wild-type (WT) and mutant (MT) pri-miR-122 and *Aequorea coerulescens* green fluorescent protein (AcGFP) were inserted between the XhoI and XbaI sites of lentiviral vector pCSII-EF-RfA, which was kindly provided by M. Hijikata, and the resulting plasmids were designated pCSII-EF-WT-miR-122, pCSII-EF-MT-miR-122, and pCSII-EF-AcGFP, respectively. Plasmids pHH-JFH1 and pSGR-JFH1, which encode full-length and subgenomic cDNA of the JFH1 strain, respectively, were kindly provided by T. Wakita. pHH-JFH1-E2p7NS2mt contains three adaptive mutations in pHH-JFH1 (53). pHH-JFH1-M1 and pHH-JFH1-M2 were established by the introduction of a point mutation of nucleotide 26 located in site 1 and nucleotide 41 in site 2 of the 5′ UTR of the JFH1 cDNA construct pHH-JFH1. pSGR-Con1, which encodes SGR of the Con1 strain, was kindly provided by R. Bartenschlager. The complementary sequences of miR-122 were introduced into the multicloning site of the pmirGLO vector (Promega, Madison, WI), and the resulting plasmid was designated pmirGLO-compl-miR-122. The plasmids used in this study were confirmed by sequencing with an ABI 3130 genetic analyzer (Applied Biosystems, Tokyo, Japan).

Cell lines. All cell lines were cultured at 37°C under the conditions of a humidified atmosphere and 5% CO_2. The following cells were maintained in Dulbecco modified Eagle medium (DMEM; Sigma-Aldrich, St. Louis, MO) supplemented with 100 U/ml penicillin, 100 μg/ml streptomycin, and 10% fetal calf serum (FCS): human hepatocellular carcinoma-derived Huh7, Hep3B, and HepG2; embryonic kidney-derived HEK293 and 293T; lung-derived RERF-LC-AI, NCI-H-2030, and A-427; kidney-derived Caki-2 and 769-P; neuron-derived MC-IXC and SK-PN-DW; uterus-derived Hec1B; ovary-derived SK-OV3; colon-derived SW620; and urinary bladder-derived SW780 cells. RERF-LC-AI (RCB0444) cells were provided by the RIKEN BRC through the National Bio-Resource Project of MEXT, Japan. Hec1B (JCRB1193) cells were obtained from the JCRB Cell Bank. NCI-H-2030, A-427, Caki-2, 769-P, MC-IXC, SK-PN-DW, SK-OV3, and SW780 cells were obtained from the American Type Culture Collection (ATCC). SW620 cells were kindly provided by C.

Oneyama. 293T-CLDN cells stably expressing CLDN1 were established by the introduction of the expression plasmids encoding CLDN1 under the control of the CAG promoter of pCAG-pm3. The Huh7-derived cell line Huh7.5.1 was kindly provided by F. Chisari. The Huh7OK1 cell line efficiently propagates HCVcc as previously described (45). Huh7, Hec1B, and HEK293 cells harboring Con1- or JFH1-based HCV SGR were prepared according to the method described in a previous report (47) and maintained in DMEM containing 10% FCS and 1 mg/ml G418 (Nakalai Tesque, Kyoto, Japan).

Antibodies and drugs. Mouse monoclonal antibodies to HCV nonstructural protein 5A (NS5A) and β-actin were purchased from Austral Biologicals (San Ramon, CA) and Sigma-Aldrich, respectively. Mouse anti-ApoE antibody was purchased from Santa Cruz Biotechnology (Santa Cruz, CA). Rabbit anti-HCV core protein and NS5A were prepared as described previously (41). Rabbit anti-SR-BI antibody was purchased from Novus Biologicals (Littleton, CO). Rabbit anti-CLDN1 and -OCLN antibodies, Alexa Fluor 488 (AF488)-conjugated anti-rabbit or -mouse IgG antibodies, and AF594-conjugated anti-mouse IgG2a antibodies were purchased from Invitrogen (San Diego, CA). Mouse anti-FKBP8 antibody was described previously (44). Mouse anti-double-stranded RNA (anti-dsRNA) IgG2a (J1 and K2) antibodies were obtained from Biocenter Ltd. (Szirak, Hungary). The HCV NS3/4A protease inhibitor was purchased from Acme Bioscience (Salt Lake City, UT). Human recombinant alpha IFN (IFN-α) and cyclosporine were purchased from PBL Biomedical Laboratories (Piscataway, NJ) and Sigma-Aldrich, respectively. BODIPY 558/568 lipid probe was purchased from Invitrogen. The locked nucleic acid (LNA) targeted to miR-122, LNA-miR-122 (5′-CcAttGTcaCaCtCC-3′), and its negative control, LNA-control (5′-CcAttCTgaCcCtAC-3′) (LNAs are in capital letters, DNAs are in lowercase letters; sulfur atoms in oligonucleotide phosphorothioates are substituted for nonbridging oxygen atoms; the capital C indicates LNA methylcytosine), were purchased from Gene Design (Osaka, Japan) (15).

Preparation of viruses. pHH-JFH1-E2p7NS2mt was introduced into Huh7.5.1 cells, HCVcc in the supernatant was collected after serial passages (39), and infectious titers were determined by a focus-forming assay and expressed in focus-forming units (FFUs) (62). Mutant HCVcc was produced from Huh7.5.1 cells expressing MT miR-122 according to the method of a previous report with minor modifications (25). HCVpv, a pseudotype vesicular stomatitis virus (VSV) bearing HCV E1 and E2 glycoproteins, was prepared as previously described (61), and infectivity was assessed by luciferase expression on a Bright-Glo luciferase assay system (Promega), following a protocol provided by the manufacturer and expressed in relative light units (RLUs).

Lipofection and lentiviral gene transduction. Cells were transfected with the plasmids by using Trans IT LT-1 transfection reagent (Mirus, Madison, WI) according to the manufacturer's protocol. LNAs were introduced into cells by Lipofectamine RNAiMAX (Invitrogen). The lentiviral vectors and ViraPower lentiviral packaging mix (Invitrogen) were cotransfected into 293T cells, and the supernatants were recovered at 48 h posttransfection. The lentivirus titer was determined by a Lenti-XTM quantitative reverse transcription-PCR (qRT-PCR) titration kit (Clontech, Mountain View, CA), and the expression levels of miR-122 and AcGFP were determined at 48 h postinoculation.

Quantitative RT-PCR. HCV RNA levels were determined by the method described previously (18). Total RNA was extracted from cells by using an RNeasy minikit (Qiagen). The first-strand cDNA synthesis and qRT-PCR were performed with TaqMan EZ RT-PCR core reagents and an ABI Prism 7000 system (Applied Biosystems), respectively, according to the manufacturer's protocols. The primers for TaqMan PCR targeted to the noncoding region of HCV RNA were synthesized as previously reported (42). To determine the expression levels of miR-122, total miRNA was prepared by using the miRNeasy minikit, and miR-122 expression was determined by using fully processed miR-122-specific RT and PCR primers provided in the TaqMan microRNA assays according to the manufacturer's protocol. U6 small nuclear RNA was used as an internal control. Fluorescent signals were analyzed with the ABI Prism 7000 system.

Immunoblotting. Cells were lysed on ice in lysis buffer (20 mM Tris-HCl [pH 7.4], 135 mM NaCl, 1% Triton X-100, 10% glycerol) supplemented with a protease inhibitor mix (Nacalai Tesque). The samples were boiled in loading buffer and subjected to 5 to 20% gradient SDS-PAGE. The proteins were transferred to polyvinylidene difluoride membranes (Millipore, Bedford, MA) and reacted with the appropriate antibodies. The immune complexes were visualized with SuperSignal West Femto substrate (Pierce, Rockford, IL) and detected with an LAS-3000 image analyzer system (Fujifilm, Tokyo, Japan).

Immunofluorescence assay. Cells cultured on glass slides were fixed with 4% paraformaldehyde (PFA) in phosphate-buffered saline (PBS) at room temperature for 30 min, permeabilized for 20 min at room temperature with PBS containing 0.2% Triton, after being washed three times with PBS, and blocked with PBS containing 2% FCS for 1 h at room temperature. The cells were incubated with PBS containing appropriate primary antibodies at room temperature for 1 h, washed three times with PBS, and incubated with PBS containing AF488- or AF594-conjugated secondary antibodies at room temperature for 1 h. For lipid droplet staining, cells incubated in medium containing 20 μg/ml BODIPY for 20 min at 37°C were washed with prewarmed fresh medium and incubated for 20 min at 37°C. Cell nuclei were stained with DAPI (4′,6-diamidino-2-phenylindole). Cells were observed with a FluoView FV1000 laser scanning confocal microscope (Olympus, Tokyo, Japan).

***In vitro* transcription, RNA transfection, and colony formation.** The plasmids pSGR-Con1 and pSGR-JFH1 were linearized with ScaI and XbaI, respectively, and treated with mung bean exonuclease. The linearized DNA was transcribed *in vitro* by using a MEGAscript T7 kit (Applied Biosystems) according to the manufacturer's protocol. The *in vitro*-transcribed RNA (10 μg) was electroporated into Hec1B and HEK293 cells at 10^7 cells/0.4 ml under conditions of 190 V and 975 μF using a Gene Pulser apparatus (Bio-Rad, Hercules, CA) and plated on DMEM containing 10% FCS. The medium was replaced with fresh DMEM containing 10% FCS and 1 mg/ml G418 at 24 h posttransfection. The remaining colonies were cloned by using a cloning ring (Asahi Glass, Tokyo, Japan) or fixed with 4% PFA and stained with crystal violet at 4 weeks postelectroporation.

Electron microscopy and correlative FM-EM analysis. Cells were cultured on a Cell Desk polystyrene coverslip (Sumitomo Bakelite) and were fixed with 2% formaldehyde and 2.5% glutaraldehyde in 0.1 M cacodylate buffer (pH 7.4) containing 7% sucrose. Cells were postfixed for 1 h with 1% osmium tetroxide and 0.5% potassium ferrocyanide in 0.1 M cacodylate buffer (pH 7.4), dehydrated in graded series of ethanol, and embedded in Epon812 (TAAB). Ultrathin (80-nm) sections were stained with saturated uranyl acetate and lead citrate solution. Electron micrographs were obtained with a JEM-1011 transmission electron microscope (JEOL). Correlative fluorescence microscopy (FM)-electron microscopy (EM) allows individual cells to be examined both in an overview with FM and in a detailed subcellular-structure view with EM (51). The NS5A was stained and observed in the Hec1B-derived Con1 SGR cells by the correlative FM-EM method as described previously (44).

Intracellular infectivity. Intracellular viral titers were determined according to a method previously reported (20). Briefly, cells were extensively washed with PBS, scraped, and centrifuged for 5 min at 1,000 × *g*. Cell pellets were resuspended in 500 μl of DMEM containing 10% FCS and subjected to three cycles of freezing and thawing using liquid nitrogen and a thermo block set to 37°C. Cell lysates were centrifuged at 10,000 × *g* for 10 min at 4°C to remove cell debris. Cell-associated infectivity was determined by a focus-forming assay.

Statistical analysis. The data for statistical analyses are averages of three independent experiments. Results were expressed as means ± standard deviations. The significance of differences in the means was determined by Student's *t* test.

Microarray data accession number. Access to data concerning this study may be found under GEO experiment accession number GSE32886.

RESULTS

Nonhepatic cell lines susceptible to HCVcc by expression of miR-122. Human CD81 (hCD81), SR-B1, CLDN1, and OCLN are crucial for HCV entry (16, 48, 49, 56). First, we examined the expression of these receptor candidates in nonhepatic cell lines by using the web-based NextBio search engine (Cupertino, CA). Multidimensional scaling was used to visualize the differences in expression patterns of molecules of various tissues, cells, and cell lines from those of hepatic cell lines and primary hepatocytes. We selected nine nonhepatic cell lines as possibly being susceptible to HCVcc infection: NCI-H-2030 (lung), Caki-2 (kidney), 769-P (bladder), A-427 (lung), SK-OV3 (ovary), SW780 (bladder), SW620 (colon), RERF-LC-AI (lung), and Hec1B (uterus) (Fig. 2). In addition, three nonhepatic cell lines previously reported to be susceptible to replication of HCV RNA—that is, SK-PN-DW (neuron), MC-IXC (neuron), and 293T-CLDN (kidney)—were included in this study (8, 17). The expression of each receptor molecule in these 12 nonhepatic cell lines was confirmed by fluorescence-activated cell sorter (FACS) analysis and immunoblotting (Fig. 3A and B). To examine the expression of the functional receptors for HCV entry in these cell lines, we inoculated HCVpv into the cells. Ten of the cell lines (A-427 and SW780 being the exceptions) exhibited various degrees of susceptibility to HCVpv infection (Fig. 3C). Therefore, we examined the possibility of propagation of HCVcc by the expression of miR-122 in these 10 cell lines.

To introduce miR-122 in the cell lines, we employed a lentiviral vector encoding pri-miR-122, an unprocessed miR-122. To confirm the maturation of pri-miR-122 to form functional RNA-induced silencing complexes (RISCs), suppression of the translation of the target mRNA was determined by a dual reporter assay. Translation of a firefly luciferase mRNA containing the sequences complementary to miR-122 in the 3′ UTR was suppressed by infection with the lentivirus encoding pri-miR-122 but not by infection with a control virus (data not shown), suggesting that the pri-miR-122 is processed into a functionally mature miR-122. By using this lentiviral vector, high levels of miR-122 expression were achieved in the 10 cell lines, comparable to the endogenous expression level of miR-122 in Huh7 cells (Fig. 4A).

To examine the effect of the exogenous expression of miR-122 on HCV replication, the nonhepatic cell lines expressing miR-122 were infected with HCVcc at a multiplicity of infection (MOI) of 1, and intracellular viral RNA was determined (Fig. 4B). The expression of miR-122 significantly increased the amount of the HCV genome in Hec1B, 293T-CLDN, MC-IXC, and RERF-LC-AI cells as well as Huh7 cells and slightly increased it in SK-OV3 and NCI-H-2030 cells. Although the levels of viral RNA in SW620, Caki-2, and SK-PN-DW cells upon expression of miR-122 were higher than those in control cells, no increase of viral RNA was observed. No effect of the expression of miR-122 was observed in 769-P cells. Interestingly, naïve Hec1B cells exhibited a delayed increase in viral RNA from 24 to 48 h postinfection, in contrast to the gradual decrease of viral RNA in other cell lines. Replication of HCV RNA in both naïve and miR-122-expressing Hec1B cells was inhibited by treatment with an inhibitor for HCV protease but not by treatment with IFN-α, due to the lack of an IFN receptor (11), whereas treatments with either IFN-α or the protease inhibitor suppressed the replication of HCV in the other cell lines expressing miR-122 (Fig. 4C). These results indicate that exogenous miR-122 expression enhances the replication of HCV even in nonhepatic cells. Hec1B cells exhibit a delayed replication of HCV, and HCV replication was enhanced by the exogenous expression of miR-122. Therefore, in this study we used Hec1B cells to investigate the biological significance of miR-122 on the replication of HCVcc in nonhepatic cells.

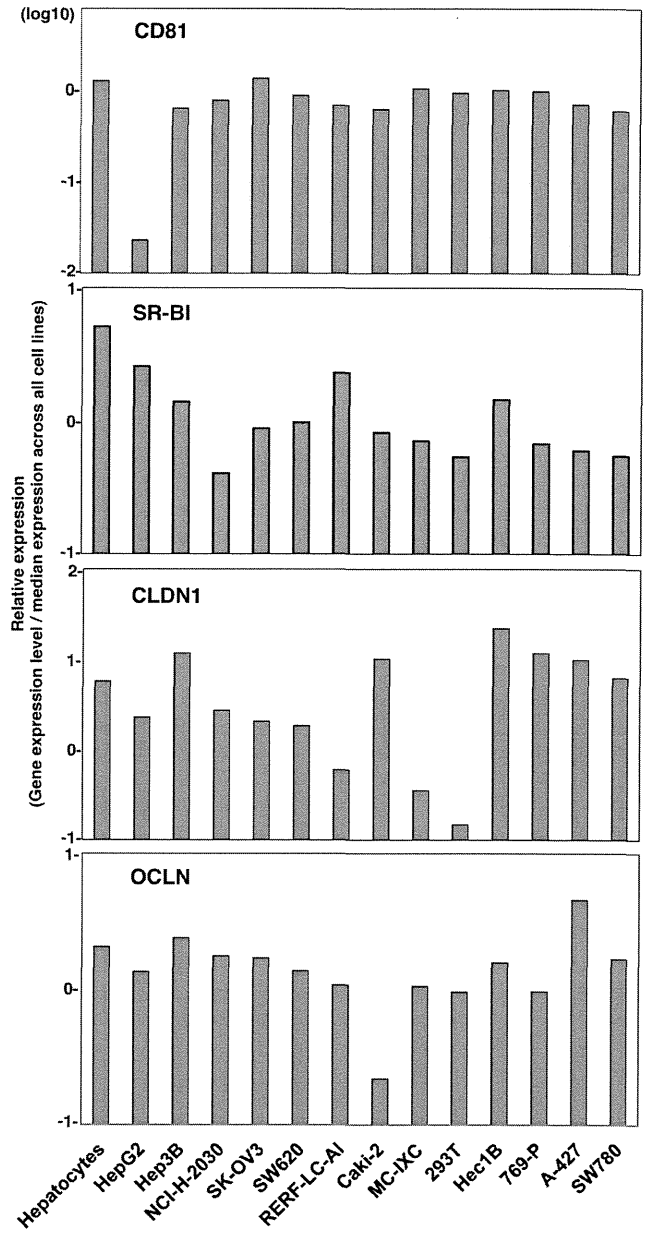

FIG 2 Receptor expression profiling in nonhepatic cells. Relative expression levels of CD81, SR-BI, CLDN1, and OCLN in primary hepatocytes, hepatic cell lines HepG2 and Hep3B, and nonhepatic cells were determined by using the NextBio Body Atlas. Expression levels were standardized by the median expression across all cell lines.

Expression of miR-122 is essential for enhancing HCV replication in Hec1B cells. To confirm the specificity of HCV replication in Hec1B cells, HCVcc was preincubated with an anti-HCV E2 monoclonal antibody, AP-33, or Hec1B/miR-122 and Hec1B/

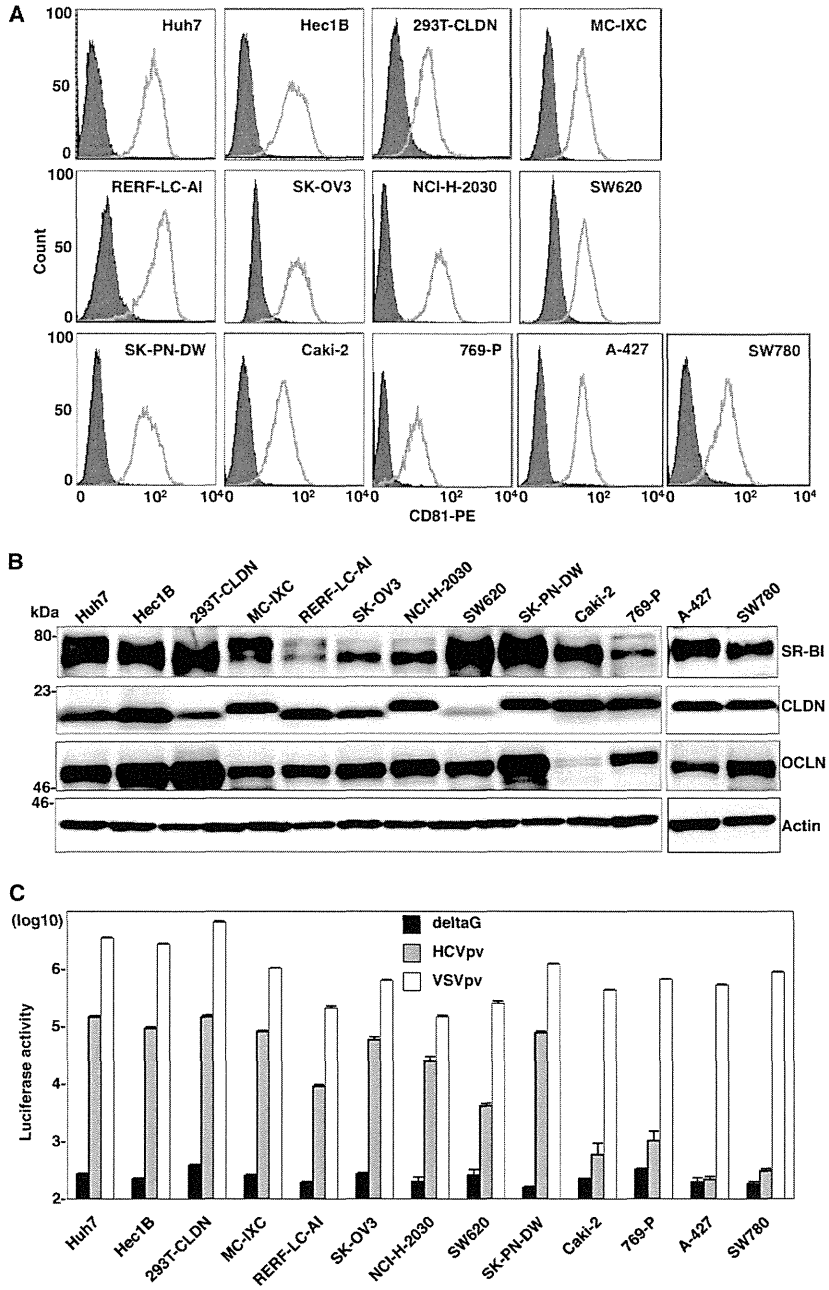

FIG 3 Expression of functional HCV receptor candidates in nonhepatic cells. (A) Expression of hCD81 in nonhepatic cells was determined by flow cytometry. PE, phycoerythrin. (B) Expression levels of SR-B1, CLDN, and OCLN in the nonhepatic cells were determined by immunoblotting. (C) The nonhepatic cell lines were inoculated with pseudotype VSVs bearing no envelope protein (deltaG), HCV envelope proteins of genotype 1b Con1 strain (HCVpv), or VSV G protein (VSVpv), and luciferase expression was determined at 24 h postinfection.

Cont cells were pretreated with anti-hCD81 monoclonal antibody. Replication of HCV RNA was determined upon infection with HCVcc. The antibody treatment significantly inhibited HCV replication in the Hec1B cell line, indicating that HCVcc internalizes into Hec1B cells through a specific interaction between hCD81 and E2 (Fig. 5). Next, we determined the dose dependence of miR-122 expression on the enhancement of HCV replication in Hec1B cells. Huh7.5.1 and Hec1B cells transduced with the lentiviral vector encoding pri-miR-122 were infected with HCVcc at an MOI of 1, and intracellular miR-122 and viral RNA were determined. Expression of miR-122 was increased in Hec1B cells in a dose-dependent manner of the lentivirus, whereas no increase was observed in Huh7.5.1 cells, probably due to the high level of endogenous expression of miR-122 (Fig. 6A, left). HCV RNA replication in Huh7.5.1 and Hec1B cells was correlated with miR-122 expression (Fig. 6A, right), suggesting a close correlation between miR-122 expression and HCV replication.

Next, we examined the expression of viral proteins in Hec1B/

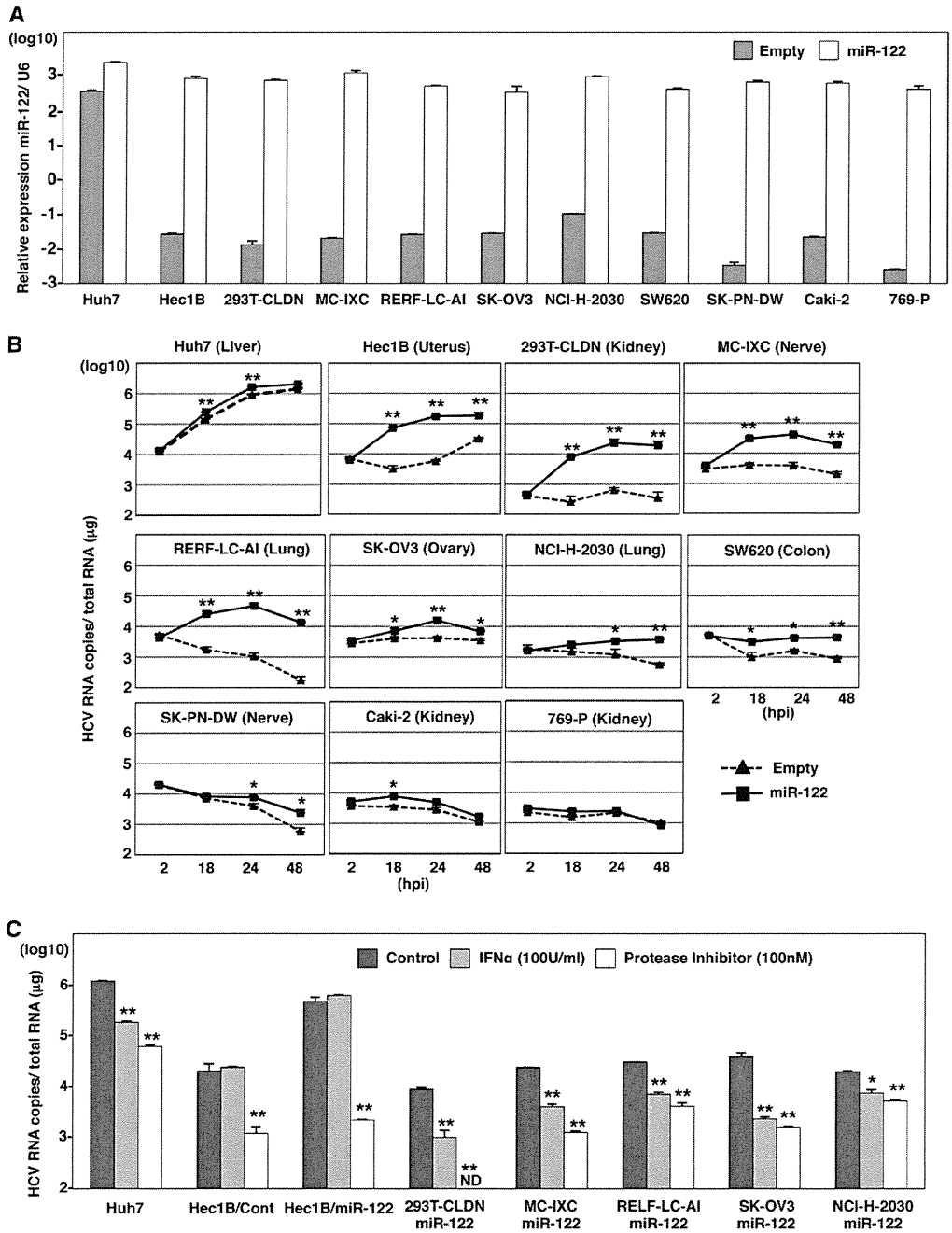

FIG 4 Nonhepatic cell lines susceptible to HCVcc by the expression of miR-122. (A) Exogenous miR-122 was expressed in Huh7, Hec1B, 293T-CLDN, MC-IXC, RERF-LC-AI, SK-OV3, NCI-H-2030, SW620, Caki-2, SK-PN-DW, and 769-P cells by lentiviral vector. Total RNA was extracted from the cells and subjected to qRT-PCR analysis. U6 was used as an internal control. Gray and white bars, endogenous and exogenous levels of miR-122, respectively. (B) HCVcc was inoculated into Huh7 and nonhepatic cell lines expressing (solid lines) or not expressing (dashed lines) exogenous miR-122 at an MOI of 1. Intracellular HCV RNA levels were determined by qRT-PCR at 2, 18, 24, and 48 h postinfection (hpi). (C) Cells were inoculated with HCVcc and simultaneously treated with either 100 U IFN-α or 100 nM HCV protease inhibitor or not treated (control), and intracellular HCV RNA levels were determined by qRT-PCR at 36 h postinfection. Asterisks indicate significant differences (*, $P < 0.05$; **, $P < 0.01$) versus the results for control cells.

miR-122 cells upon infection with HCVcc by immunoblotting and fluorescence microscopic analyses (Fig. 6B). Expression of NS5A protein was increased in Hec1B/miR-122 cells in an MOI-dependent manner. Expression of NS5A in Hec1B/Cont cells infected with HCVcc at an MOI of 3 was significantly lower than that in Hec1B/miR-122 cells infected with HCVcc at an MOI of 0.5. HCV core and NS proteins were shown to localize mainly on the lipid droplets and cytoplasmic face of the endoplasmic reticulum (ER) in Huh7 and Hep3B/miR-122 cells infected with HCVcc (29, 40). Immunofluorescence analyses revealed that HCV core and NS5A proteins were colocalized with lipid droplets and calnexin, an ER marker, in Hec1B cells infected with HCVcc (Fig. 7).

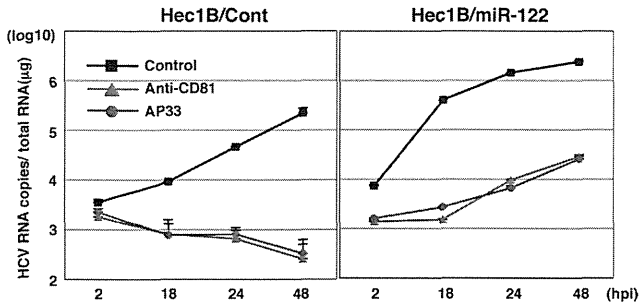

FIG 5 Neutralization of HCVcc infection in Hec1B cells by specific antibodies. HCVcc was preincubated with anti-E2 antibody (AP-33) and inoculated into Hec1B/Cont and Hec1B-miR-122 cells. Cells were preincubated with anti-human CD81 antibody and inoculated with HCVcc. Intracellular HCV RNA levels at 2, 18, 24, and 48 h postinfection were determined by qRT-PCR.

To further confirm the specificity of the enhancement of HCV replication by the expression of miR-122, Huh7, Hec1B/miR-122, and Hec1B/Cont cells were treated with LNAs that were either specific to miR-122 (LNA-miR-122) or nonspecific (LNA-control) at 6 h before infection with HCVcc. Although the treatment with LNA-miR-122 inhibited the enhancement of viral RNA replication in Huh7 and Hec1B/miR-122 cells in a dose-dependent manner, no inhibition of viral replication was observed in Hec1B/Cont cells (Fig. 6C). These results suggest that Hec1B cells permit HCV replication in a miR-122-independent manner and exogenous expression of miR-122 enhances viral replication.

Specific interaction between miR-122 and the 5′ UTR of HCV is required for HCV replication. To determine the effect of the specific interaction between miR-122 and the 5′ UTR of the HCV genome on the enhancement of RNA replication, we generated MT pri-miR-122 carrying a substitution of uridine to adenosine in the seed domain and an additional complementary substitution of adenosine to uridine to stabilize the loop structure of pri-miR-122 (Fig. 8A). A high expression level of MT miR-122, comparable to that of WT miR-122, was introduced into Hec1B cells by infection with lentiviral vectors (Fig. 8B). To determine the specificity of miR-122 on the replication of HCV, Hec1B cells expressing either WT or MT miR-122 were inoculated with HCVcc at an MOI of 1. Enhancement of HCV replication was observed in Hec1B cells by the expression of WT but not that of MT miR-122, suggesting that the sequence specificity of miR-122 with the 5′ UTR of HCV is crucial for the efficient replication of HCV (Fig. 8C). To further confirm the effect of the specificity of interaction between miR-122 and the binding sites in the 5′ UTR of HCV on the enhancement of HCV replication, we generated two mutant viruses, HCVcc-M1 and HCVcc-M2, carrying complementary substitutions in the miR-122-binding site 1 alone and in both sites 1 and 2 in the 5′ UTR of HCV, respectively (Fig. 8D). Recently, Jangra et al. demonstrated that the propagation of a mutant HCVcc bearing mutations in sites 1 and 2 in the 5′ UTR was rescued by the expression of MT miR-122 in Huh7.5 cells (25). We confirmed that the propagation of HCVcc-M1 and HCVcc-M2 in Huh7.5.1 cells was rescued by the expression of MT miR-122 but not of WT miR-122, although the recovery of infectious titers of HCVcc-M2 was significantly lower than the recovery of infectious titers of HCVcc-M1 (Fig. 8E). Next, to examine the interaction between miR-122 and the HCV genome in Hec1B cells, we inoculated HCVcc or mutant viruses into Hec1B cells expressing either or both WT and MT miR-122 and determined the replication of HCV RNA by qRT-PCR (Fig. 8F). Expression of WT and MT miR-122 in Hec1B cells permits replication of HCVcc and HCVcc-M2, respectively, although the enhancing effects differed. On the other hand, the expression of both WT and MT miR-122 is required for the replication of HCVcc-M1, because MT and WT miR-122 bind to sites 1 and 2 in the 5′ UTR of this virus, respectively. Interestingly, a low level of HCVcc-M1 replication was also observed in Hec1B cells expressing either WT or MT miR-122, in contrast to the requirement of the corresponding miR-122 for the replication of HCVcc and HCVcc-M2. These results suggest that the specific interaction between miR-122 and the 5′ UTR of HCV is crucial for the replication of HCV.

Viral particle formation in hepatic and nonhepatic cells. These data suggest that miR-122 expression facilitates replication of HCV RNA in nonhepatic cells. Recently, we have shown that expression of miR-122 facilitates infectious particle formation of HCVcc in a hepatoma cell line, Hep3B (29). To examine the effect of miR-122 expression on particle formation in nonhepatic cells, intracellular and extracellular viral RNA levels in cells infected with HCVcc were determined. Intracellular RNA replication in the hepatic cell lines, including Huh7.5.1 and Hep3B/miR-122, was increased up to 72 h postinfection with HCVcc, whereas in nonhepatic cell lines, including 293T-CLDN/miR-122 and Hec1B/miR-122, such replication was comparable to that in the hepatic cell lines until 24 h postinfection but reached a limit at this point (Fig. 9A). In spite of no clear increase of intracellular HCV RNA in Hep3B/Cont cells upon infection with HCVcc (Fig. 9A), subtle but substantial production of infectious particles was detected in the culture supernatants at 72 h postinfection, in contrast to no production of infectious particles in those of the nonhepatic cell lines (Fig. 9B). Furthermore, no focus formation was observed in Hec1B/miR-122 cells upon infection with HCVcc, in contrast to the many foci in Huh7.5.1 cells (Fig. 9C), and no infectivity was detected even in the lysates of Hec1B/miR-122 cells infected with HCVcc (Fig. 9D). These results suggest that not only the replication efficiency of viral RNA but also other factors are involved in the assembly of HCV and that the viral assembly process is impaired in Hec1B/miR-122 cells infected with HCVcc, in spite of the efficient replication of HCV RNA.

It was previously shown that lipid droplets, diacylglycerol *O*-acyltransferase 1 (DGAT1), and apolipoproteins B and E play an important role in the assembly of HCV particles (10, 22, 40). To understand the molecular mechanisms underlying the low efficiency of infectious particle formation in nonhepatic cells, we first examined the subcellular localization of lipid droplets and HCV core protein in Hec1B/miR-122 cells infected with HCVcc. Although the core protein was detected around the lipid droplets, as seen in Huh7.5.1 cells, only a small amount of lipid droplets was detected in Hec1B/miR-122 cells infected with HCVcc compared with the amount detected in Huh7.5.1 cells (Fig. 9E), suggesting that the low level of lipid droplet formation is involved in the impairment of infectious particle formation in nonhepatic cells.

Next we examined the expression patterns of molecules involved in lipid metabolism by using cDNA microarray and qPCR analyses. Although expression levels of low-density lipoprotein receptor (LDLR), sterol regulatory element-binding protein 1c (SREBP1c), SREBP2, and DGAT1 in nonhepatic Hec1B and 293T cells were comparable to those in hepatic Huh7 and Hep3B cells, those of VLDL-associated proteins, including ApoE, ApoB, and

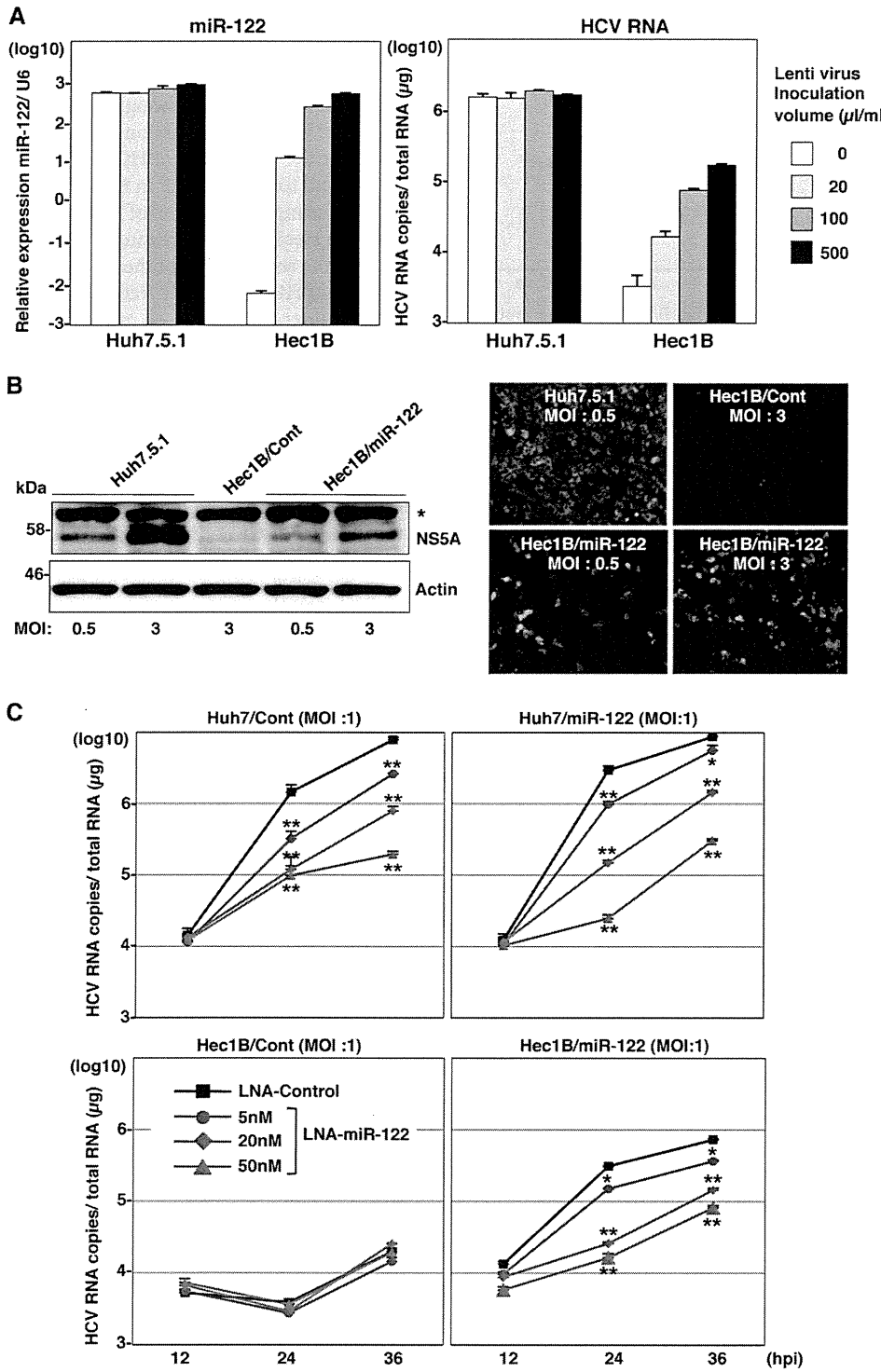

FIG 6 Expression of miR-122 is essential for the enhancement of HCV replication in the Hec1B cells. (A) Huh7.5.1 and Hec1B cells were transduced with lentiviral vectors expressing miR-122 in a dose-dependent manner and infected with HCVcc at an MOI of 1. Intracellular miR-122 and HCV RNA were determined at 24 h postinfection by qRT-PCR. (B) Huh7.5.1 and Hec1B/miR-122 cells were infected with HCVcc at an MOI of 0.5 or 3 and subjected to immunoblotting and immunofluorescence analyses using anti-NS5A antibodies at 48 h postinfection. The asterisk indicates nonspecific bands. (C) LNAs specific to miR-122 at a final concentration of 5 nM, 20 nM, or 50 nM and control (LNA alone at 50 nM) were introduced into Huh7/Cont, Huh7/miR-122, Hec1B/miR-122, and Hec1B/Cont cells by using Lipofectamine RNAiMAX transfection reagent and infected with HCVcc at an MOI of 1 at 6 h posttransfection. Intracellular HCV RNA levels were determined by qRT-PCR at 12, 24, and 36 h postinfection. Asterisks indicate significant differences (*, $P < 0.05$; **, $P < 0.01$) versus the results for control cells.

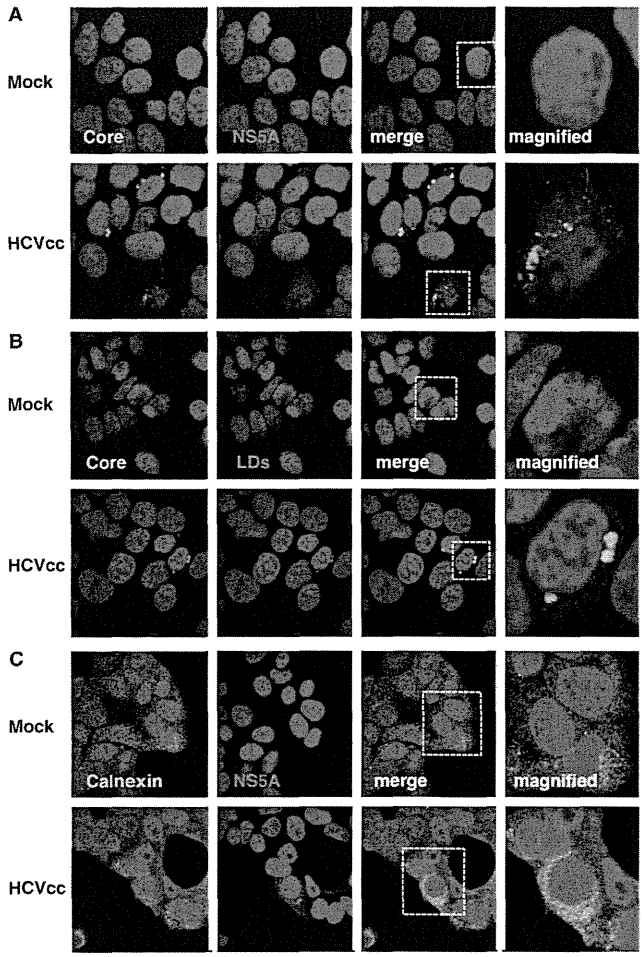

FIG 7 Subcellular localization of core and NS5A proteins in Hec1B/miR-122 cells infected with HCVcc. Hec1B/miR-122 cells infected with or without HCVcc at an MOI of 1 were fixed with 4% PFA at 48 h postinfection and stained with appropriate antibodies to core and NS5A proteins (A), core protein and lipid droplets (B), and NS5A and calnexin (C). The boxes in the merged images were magnified, and the images are displayed on the right.

MTTP, in nonhepatic cells were significantly lower than those in hepatic cells (Fig. 10). Collectively, these results suggest that intracellular functional lipid metabolism, including the biosynthesis of lipid droplets and the production of VLDL, participates in the assembly of HCV.

Establishment of HCV replicon in Hec1B/miR-122 cells. It was previously shown by using RNA replicon cells based on the JFH1 strain that expression of miR-122 enhanced the translation of HCV RNA in HEK293 cells and MEFs (8, 35). We tried to establish HCV replicon cells based on genotype 1b Con1 and genotype 2a JFH1 strains in Hec1B/miR-122 and HEK293 cells stably expressing miR-122 (HEK293/miR-122). To examine the colony formation efficiency of the HCV RNAs of the Con1 and JFH1 strains, SGR RNA was electroporated into the cell lines and selected by G418 for 3 weeks. Expression of miR-122 in Hec1B cells significantly enhanced the colony formation of SGR of the Con1 strain (Fig. 11A), suggesting that the expression of miR-122 in Hec1B cells supports the efficient replication of SGR. HCV replication in 20 replicon clones established by the transfection with SGR RNA of the Con1 strain in Hec1B/miR-122 cells was examined by qRT-PCR and immunoblotting. All clones contained high levels of HCV RNA (3×10^6 to 5×10^7 copies per μg of total RNA) (Fig. 11B), and expression of NS5A was well correlated with the levels of HCV RNA in the clones (Fig. 11C). Two replicon clones (clones 2 and 10) in Hec1B/miR-122 cells exhibiting high levels of RNA replication and NS5A expression further confirmed the high level of expression of NS5A by immunofluorescent microscopy (Fig. 11D). These results suggest that expression of miR-122 facilitates the efficient replication of SGR of at least two HCV genotypes in Hec1B cells.

Our previous reports showed that HCV NS proteins were colocalized with dsRNA and cochaperone molecules, FK506-binding protein 8 (FKBP8), in dot-like structures on the ER membrane of Huh7 replicon cells (59). Colocalization of NS5A with dsRNA or FKBP8 was observed in the dot-like structures in not only Huh7 SGR cells but also Hec1B/miR-122 SGR cells (Fig. 12A), suggesting that the dot-like structure required for efficient viral replication is also generated in Hec1B/miR-122 replicon cells. It has been shown that HCV replication induces the formation of convoluted membranous structures, called membranous webs, in Huh7 cells (13, 45). FM-EM techniques revealed the localization of NS5A on the convoluted structures in Hec1B/miR-122 replicon cells (Fig. 12B). These results suggest that the replication complex required for viral replication was also generated in the Hec1B/miR-122 replicon cells, as was seen in the Huh7 replicon cells.

miR-122 is a crucial determinant of HCVcc propagation. It has been shown that the infectivity of HCVcc in cured cells, established when IFN treatment induces the elimination of the viral genome from the Huh7 replicon cells harboring an HCV RNA, is significantly higher than that in parental Huh7 cells (2, 66). Therefore, we tried to establish Hec1B-based cured cells from the Con1 SGR clones harboring a high copy number of HCV RNA. Treatment with cyclosporine and the protease inhibitor of HCV suppressed NS5A expression in Hec1B/miR-122 SGR clone 2 in a dose-dependent manner (Fig. 13A), whereas no reduction was observed by the IFN treatment due to a lack of an IFN receptor, as shown in Fig. 4C. It was reported that monotherapy by the HCV protease inhibitor induces the emergence of resistant breakthrough viruses (34, 55). Therefore, we treated five Hec1B/miR-122 SGR clones (clones 2, 5, 10, 14, and 16) with 1 μg/ml cyclosporine and 100 nM protease inhibitor for HCV. Viral RNA was determined by qRT-PCR every 5 days posttreatment. Elimination of viral RNA was achieved in four clones (clones 2, 5, 10, and 14) within 20 days posttreatment (Fig. 13B). Replication of HCV RNA in the cured cells infected with HCVcc at an MOI of 0.5 was 2- to 30-fold higher than that in parental cells at 24 h postinfection (Fig. 13C). In addition, replication of HCV RNA in cured clone 2 infected with HCVcc at an MOI of 0.1 was comparable to that in Huh7.5.1 cells until 24 h postinfection (Fig. 13D). Expression of NS5A was significantly increased in cured clone 2 compared to that in the parental Hec1B/miR-122 cells (Fig. 13E and F). It was previously shown that the increased permissiveness of Huh7-derived cured cells, Huh7.5 cells, is attributable to a mutation in the RIG-I gene (58). To examine the innate immune response in the parental and cured Hec1B/miR-122 cells, induction of IFN-stimulated gene 15 (ISG15) was determined upon stimulation with IFN-α or VSV. Although induction of ISG15 was not observed in either parental or cured cells upon stimulation with IFN-α due to a lack of an IFN receptor (11) (Fig. 14A), it was

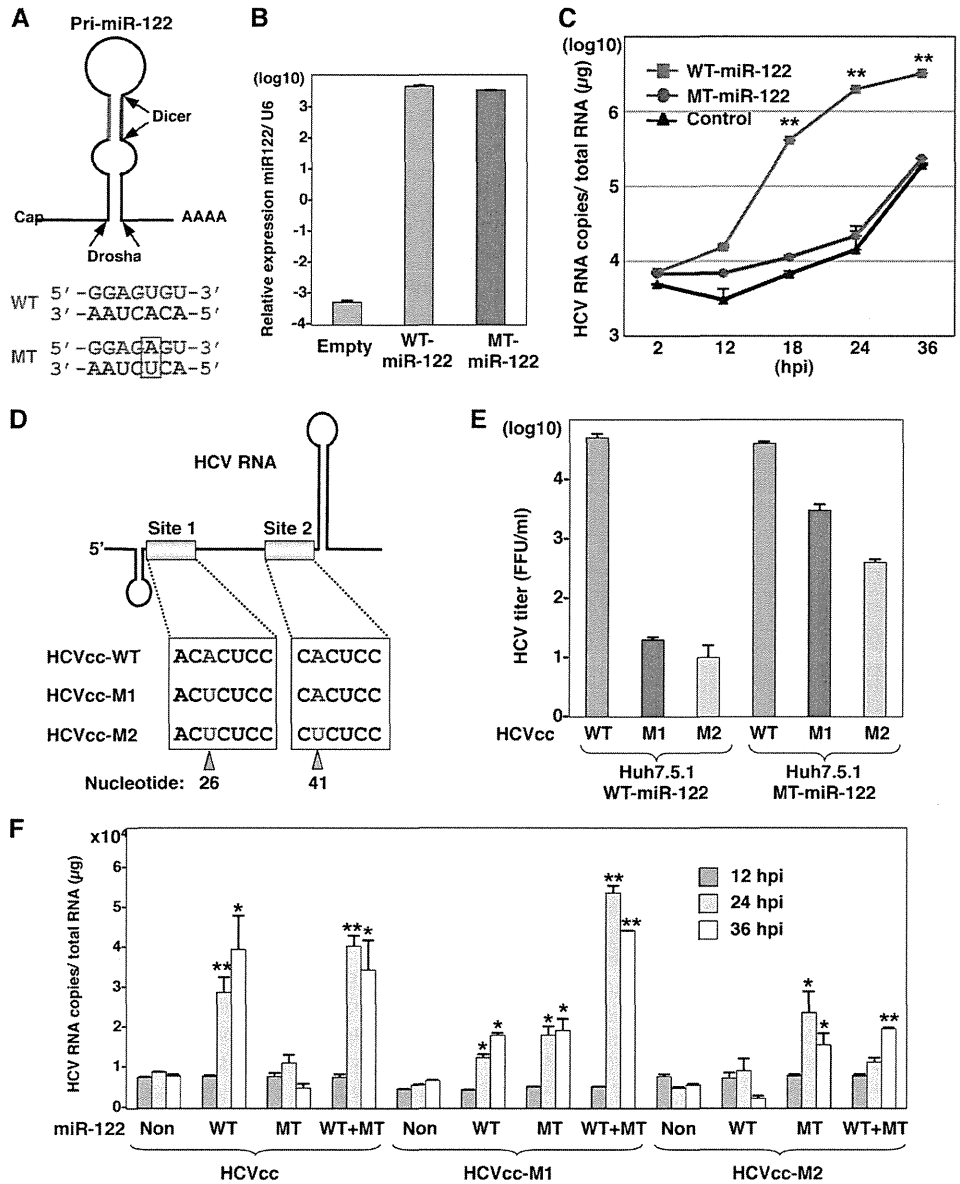

FIG 8 Specific interaction between miR-122 and the 5′ UTR of HCV is required for HCV replication. (A) Structures of pri-miR-122 and the nucleotide sequences of WT and MT miR-122, which has a substitution of uridine to adenosine in the seed domain and an additional complementary substitution of adenosine to uridine for stable expression. (B) WT or MT miR-122 was introduced into Hec1B cells by a lentiviral vector, and miR-122 expression levels were determined by qRT-PCR. (C) HCVcc was inoculated into Hec1B cells expressing either WT or MT miR-122 and control cells at an MOI of 1, and the intracellular HCV RNA levels were determined by qRT-PCR. (D) Diagram of mutant viruses HCVcc-M1 and HCVcc-M2 carrying complementary substitutions in the miR-122-binding site 1 alone and both sites 1 and 2 in the 5′ UTR of HCV, respectively. (E) Viral RNA of HCVcc, HCVcc-M1, or HCVcc-M2 was electroporated into Huh7.5.1 cells expressing either WT or MT miR-122, and infectious titers of the viruses recovered in the culture supernatants at 72 h postinfection of the second passage were determined by a focus-forming assay in cells expressing either WT or MT miR-122. Red, blue, and green bars, infectious titers of HCVcc, HCVcc-M1, and HCV-M2, respectively. (F) HCVcc, HCVcc-M1, or HCV-M2 was inoculated into Hec1B cells expressing either or both WT and MT miR-122 at an MOI of 0.5, and intracellular HCV RNA levels were determined at 12, 24, and 36 h postinfection by qRT-PCR. Asterisks indicate significant differences (*, $P < 0.05$; **, $P < 0.01$) versus the results for control cells.

detected in both cells infected with VSV (Fig. 14B). Therefore, other mechanisms should be involved in the enhancement of permissiveness of Hec1B-derived cured cells. Ehrhardt et al. showed that the expression levels of miR-122 in Huh7-derived cured cells, including Huh7.5, Huh7.5.1, and Huh7-Lunet cells, are significantly higher than those in parental Huh7 cells (14). In addition, our recent study indicated that levels of expression of miR-122 in the cured Huh7 and Hep3B/miR-122 cells were higher than those in parental cells (29). Levels of expression of miR-122 in the Hec1B-based cured cell clones are also higher than those in parental Hec1B/miR-122 cells (Fig. 13G). These results suggest that a high level of miR-122 expression is a crucial determinant of high susceptibility to HCVcc propagation in the cured cells.

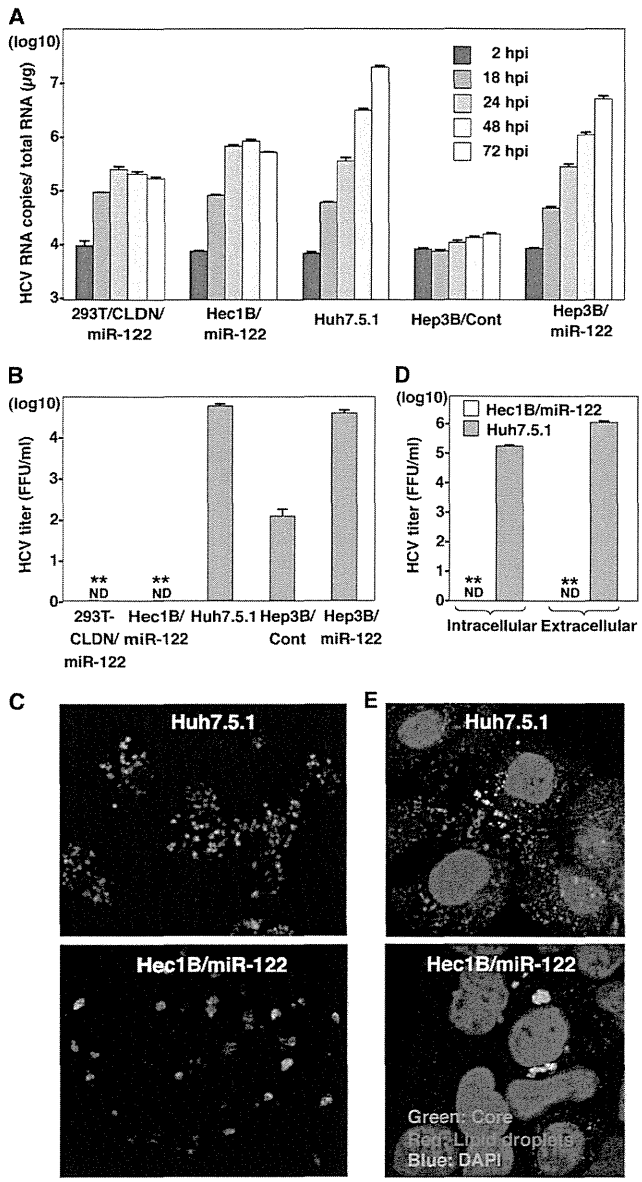

FIG 9 Viral particle formation in hepatic and nonhepatic cells. (A) HCVcc was inoculated into 293T-CLDN/miR-122, Hec1B/miR-122, Hep3B/Cont, and Hep3B/miR-122 cells at an MOI of 1 and into Huh7.5.1 cells at an MOI of 0.1. HCV RNA levels (copies/μg) in cells at 2, 18, 24, 48, and 72 h postinfection were determined by qRT-PCR. (B) HCVcc was inoculated into 293T-CLDN/miR-122, Hec1B/miR-122, Hep3B/Cont, and Hep3B/miR-122 cells at an MOI of 1 or into Huh7.5.1 cells at an MOI of 0.1, and infectious titers in the culture supernatants were determined at 72 h postinfection by a focus-forming assay in Huh7.5.1 cells. ND, not determined. (C) Huh7.5.1 and Hec1B/miR-122 cells were infected with HCVcc at MOIs of 0.1 and 1, respectively, incubated with 1% methylcellulose in DMEM containing 10% FCS for 72 h, fixed with 4% PFA, and subjected to immunofluorescence analysis using anti-NS5A antibody. (D) Hec1B/miR-122 and Huh7.5.1 cells were infected with HCVcc at MOIs of 1 and 0.1, respectively, and infectious titers in cells and supernatants were determined by a focus-forming assay at 72 h postinfection. (E) Huh7.5.1 and Hec1B/miR-122 cells were infected with HCVcc at MOIs of 0.1 and 1, respectively, fixed with 4% PFA, and subjected to immunofluorescence assay using anti-core protein antibody (green). Lipid droplets and cell nuclei were stained with BODIPY (red) and DAPI (blue), respectively. Asterisks indicate significant differences (**, $P < 0.01$) versus the results for Huh7.5.1 cells.

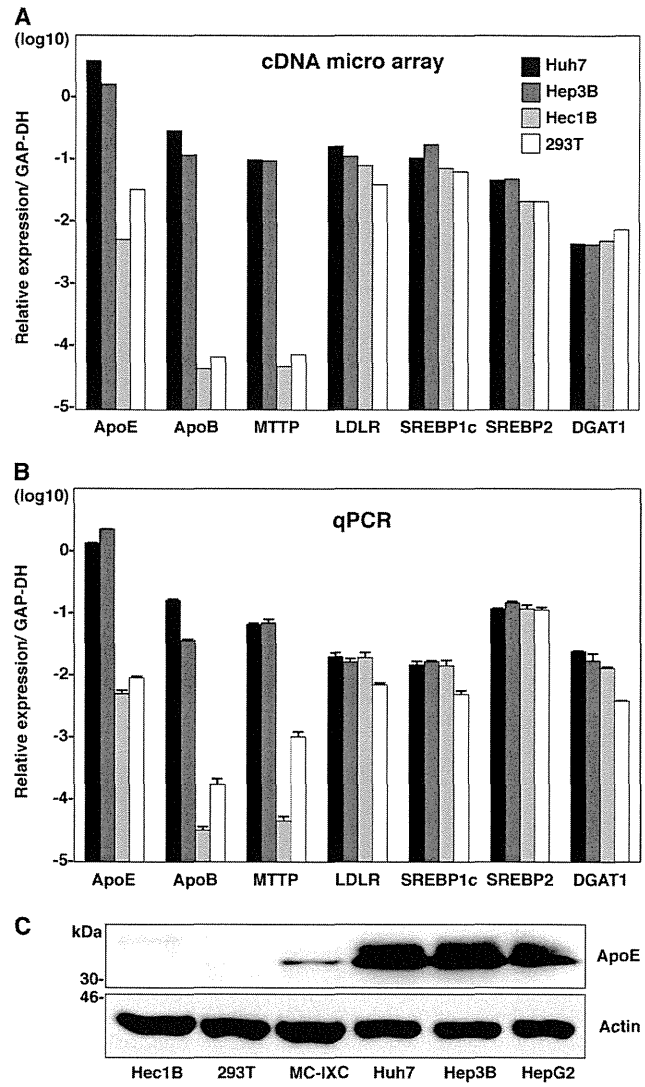

FIG 10 Expression of lipid metabolism-associated proteins in hepatic and nonhepatic cells. (A) Expression levels of ApoE, ApoB, MTTP, LDLR, SREBP1c, SREBP2, and DGAT1 were compared among hepatic (Huh7 and Hep3B) and nonhepatic (Hec1B and 293T) cells using cDNA microarray analyses. (B) Total RNA was extracted from the cells, and expression levels of ApoE, ApoB, MTTP, LDLR, SREBP1c, SREBP2, and DGAT1 gene were determined by qPCR. (C) Nonhepatic (Hec1B, 293T, and MC-IXC) and hepatic (Huh7, Hep3B, and HepG2) cells were subjected to immunoblotting using anti-ApoE antibody.

DISCUSSION

Although multiple epidemiological studies have revealed that HCV infection induces several EHMs, they have not well elucidated the molecular mechanisms of the EHMs induced by HCV infection (19). Indeed, HCVcc does not infect PBMCs (38). It has been shown that two neuroepithelioma cell lines permit HCVcc infection at low levels (17) and lymphotropic strains or quasispecies of HCV exist in infected individuals (12, 52). Furthermore, many molecules involved in the entry, replication, and assembly of HCVcc have been identified, although these molecules are not sufficient to explain the liver tropism of HCV. Recently, a liver-specific microRNA, miR-122, was shown to facilitate the efficient

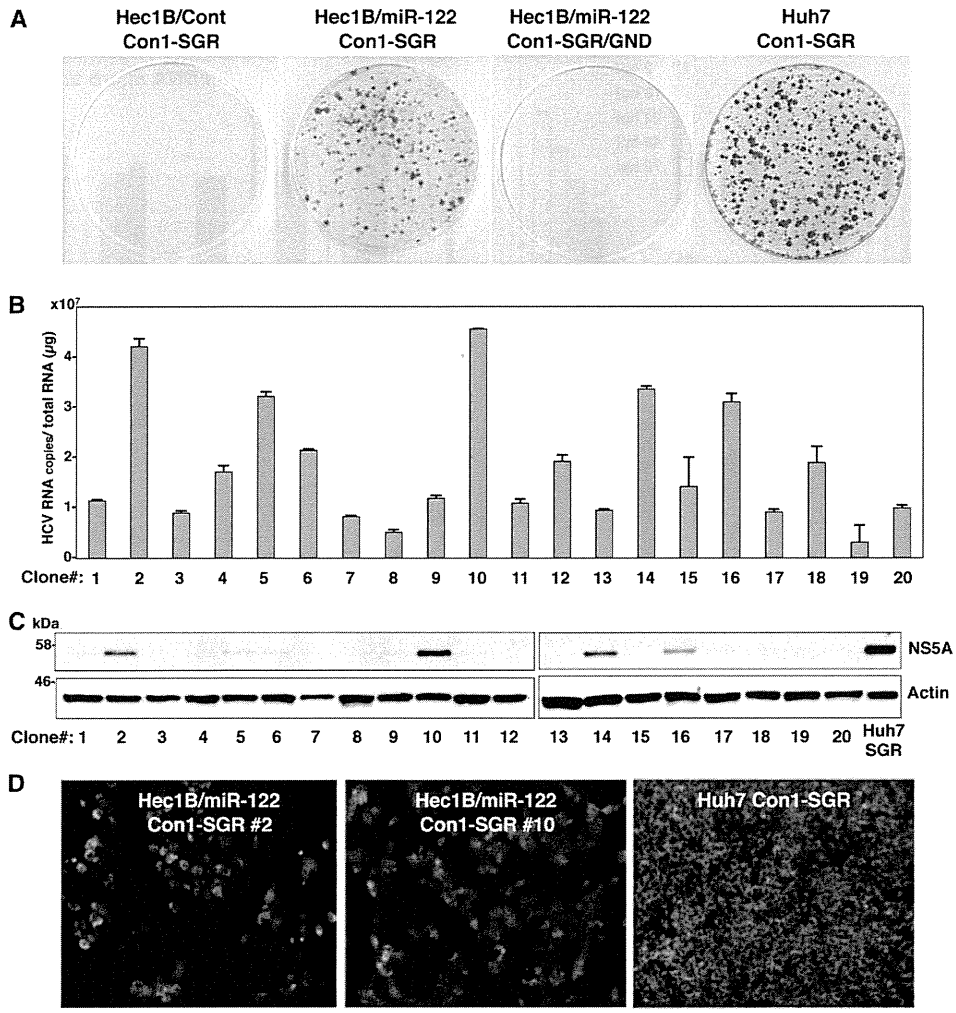

FIG 11 Establishment of Con1-based HCV replicon cells by using Hec1B cells. (A) WT or replication-defective SGR RNA of the HCV Con1 strain was electroporated into Hec1B/Cont, Hec1B/miR-122, and Huh7 cells, and the medium was replaced with DMEM containing 10% FCS and 1 mg/ml G418 at 24 h postelectroporation. Colonies were stained with crystal violet after 3 weeks of selection with G418. (B) Total RNAs of 20 selected clones were extracted and subjected to qRT-PCR. (C) The 20 SGR clones were subjected to immunoblotting using anti-NS5A antibody. Huh7-derived Con1-based SGR cells were used as a positive control. (D) NS5A proteins in SGR clones 2 and 10 were stained with appropriate antibodies and examined by fluorescence microscopy. Huh7-derived Con1-based SGR and parental Hec1B cells were used for positive and negative controls, respectively.

replication of HCV through a specific interaction with the complementary sequences in the 5′ UTR of HCV RNA (21, 25, 27, 36). In addition, exogenous expression of miR-122 facilitates the replication of SGR of the JFH1 strain in HEK293 cells (8) and the propagation of HCVcc in HepG2 and Hep3B nonpermissive hepatoma cells (29, 43), suggesting that the expression of miR-122 is required for the efficient replication of HCV. However, HCV replicon cells have also been established in HeLa and LI90 cells derived from stellate cells in which no exogenous miR-122 is expressed (30, 63). In this study, naïve Hec1B cells also exhibited a low level of replication upon infection with HCVcc (Fig. 4B), and this replication was resistant to treatment with an inhibitor of miR-122, LNA-miR-122 (Fig. 6C), suggesting that miR-122 expression is not a necessary condition but is required for the enhancement of HCV replication and that HCV is capable of replicating in nonhepatic cells in an miR-122-independent manner. Although the application of miR-122-specific LNAs to chronic hepatitis C patients is now in progress (32), further studies are needed to clarify the mechanisms underlying the miR-122-independent replication of HCV in more detail.

Although the importance of receptor-mediated entry in the cell tropism of HCV has been evaluated (16, 65), cDNA microarray databases, including the NextBio search engine, revealed that HCV receptor candidates, including hCD81, SR-BI, CLDN1, and OCLN, are highly expressed in many nonhepatic tissues. In addition, our current data and previous reports demonstrated that many nonhepatic cells permitted the entry of the pseudotype viruses bearing HCV envelope proteins, suggesting that other host factors must be involved in the cell tropism of HCV to human hepatocytes (4, 17, 54, 61). The data in this study suggest that miR-122 expression and functional lipid metabolism play crucial roles in the determination of an efficient propagation of HCV *in vitro*. On the other hand, previous studies showed the compartmentalization of genetic variation in HCV between hepatic and

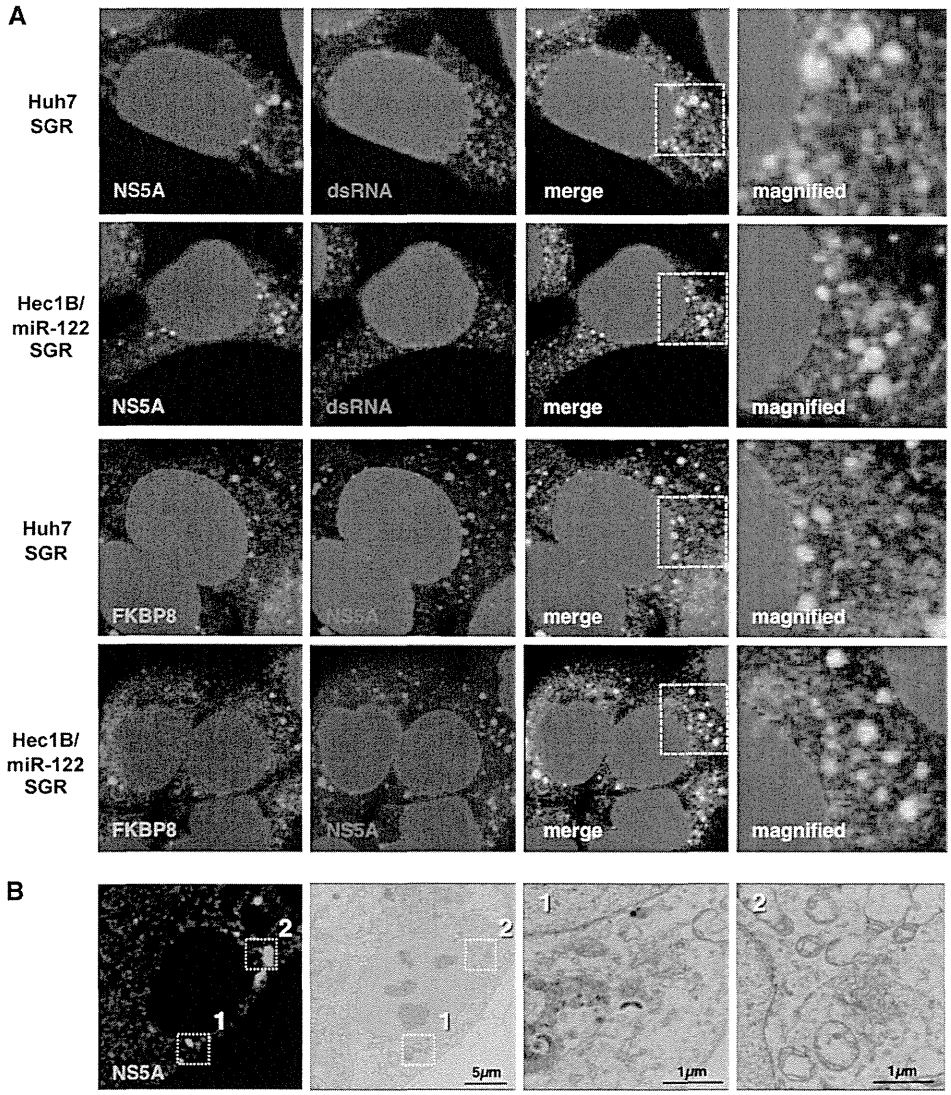

FIG 12 Replication complex in Hec1B/miR-122 replicon cells. (A) Huh7 and Hec1B/miR-122 cells harboring the Con1 SGR RNA were fixed, permeabilized, and stained with antibodies to NS5A and dsRNA or FKBP8. The boxed areas in the merged images were magnified, and the images are displayed on the right. (B) Hec1B-derived Con1 SGR cells were stained with anti-NS5A antibody. Identical fields were observed under EM by using the correlative FM-EM technique. The boxed areas are magnified, and the images displayed on the right.

nonhepatic tissues, suggesting that HCV is capable of replicating in nonhepatic tissues expressing either miR-122, ApoE, ApoB, or MTTP (52). Collectively, these results suggest that entry receptors, miR-122, and functional lipid metabolism are mainly involved in the regulation of internalization, RNA replication, and assembly of HCV, respectively, and are important factors in determining the cell tropism of HCV to hepatocytes. On the other hand, it might be feasible to speculate that EHMs observed in chronic hepatitis C patients are caused by an incomplete miR-122-independent propagation of HCV in nonhepatic cells.

In spite of the efficient replication of HCV in Hec1B and 293T-CLDN cells expressing miR-122, no infectious particle was detected, in contrast to the case with hepatic cells (Fig. 9), suggesting the involvement of liver-specific host factors and/or machineries in the assembly of infectious particles. In general, the liver plays a major role in lipid metabolism, such as in fatty acid and lipoprotein syntheses (9), and many reports have indicated the involvement of lipid metabolism, especially triglyceride metabolism, in the assembly and budding of HCV particles. Lipid droplets, MTTP, ApoB, and ApoE have been shown to participate in the assembly and secretion of infectious particles of HCVcc in Huh7 cells (20, 23, 26, 40). In the current analyses, there were fewer lipid droplets and the expression levels of ApoE, ApoB, and MTTP were lower in nonhepatic cells than in hepatic cells. Although minus-strand HCV RNA and viral proteins were detected in nonhepatic cells (33, 60), it was shown that the recurrence of HCV after liver transplantation for patients with HCV-induced liver diseases was mainly caused by HCV variants generated in the liver but not in nonhepatic tissues (50). These results support the notion that replication of HCV RNA in nonhepatic cells is unlikely to be a reservoir for persistent infection, due to the lack of infectious particle formation.

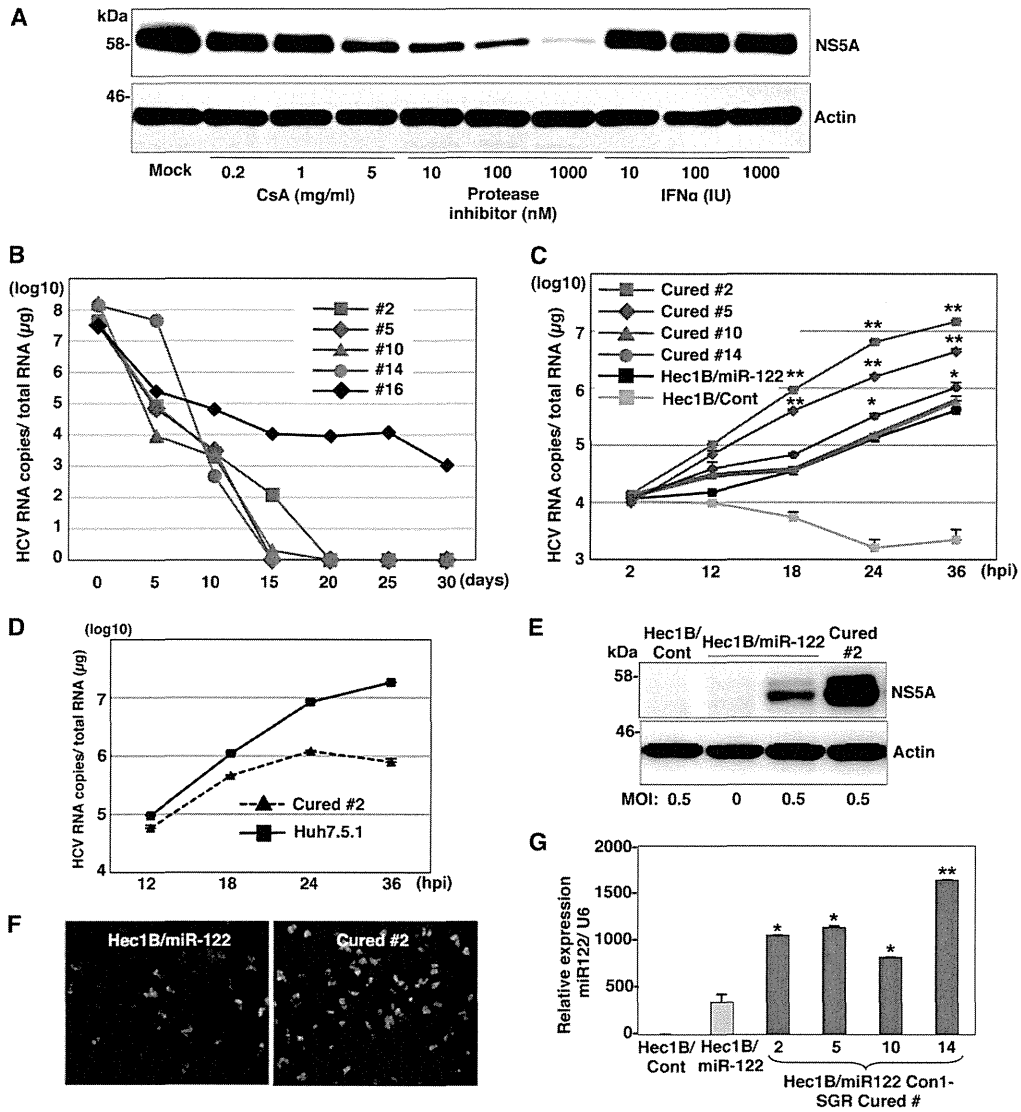

FIG 13 miR-122 is a crucial determinant for the efficient replication of HCVcc and replicon RNA. (A) Hec1B Con1 replicon clone 2 was treated with stepwise concentrations of cyclosporine (CsA; 0.2, 1, and 5 μg/ml), NS3/4A protease inhibitor (10, 100, and 1,000 nM), or IFN-α (10, 100, and 1,000 IU) and subjected to immunoblotting using anti-NS5A antibody at 48 h posttreatment. (B) Five Con1-based SGR clones were treated with the combination of 1 μg/ml cyclosporine and 100 nM HCV protease inhibitor to eliminate the HCV genome. Intracellular HCV RNA levels at 5, 10, 15, 20, 25, and 30 days posttreatment were determined by qRT-PCR analysis. (C) HCVcc was inoculated with Hec1B/Cont, parental Hec1B/miR-122, and Hec1B-based cured cells (clones 2, 5, 10, and 14) at an MOI of 1. Intracellular HCV RNA levels at 2, 12, 18, 24, and 36 h postinfection were determined by qRT-PCR analysis. (D) HCVcc was inoculated into Huh7.5.1 and Hec1B/miR-122 cured clone 2 cells at an MOI of 1. Intracellular HCV RNA levels were determined by qRT-PCR at 12, 24, 36, and 48 h postinfection. (E and F) Hec1B/Cont, parental Hec1B/miR-122, and cured cells of clone 2 were infected with HCVcc at an MOI of 0.5. After 48 h, the cells were subjected to immunoblotting and immunofluorescence analyses using appropriate antibodies. (G) Total miRNAs were extracted from Hec1B/Cont (white), parental Hec1B-miR-122 cells (gray), and four cured cell clones (black). miR-122 expression levels in these cells were determined by qRT-PCR analysis. Asterisks indicate significant differences (*, $P < 0.05$; **, $P < 0.01$) versus the results for parental Hec1B/miR-122 cells.

The endogenous expression of miR-122 is hardly detected in Hec1B cells, in contrast to the abundant expression of miR-122 in Huh7 cells. Therefore, more accurate analyses of the biological significance of the interaction between miR-122 and the 5′ UTR on the replication of HCVcc in Hec1B could be possible by introducing mutations not only into viruses but also into miR-122. Replication of HCVcc and a mutant virus bearing two mutations in the 5′ UTR (HCVcc-M2) was observed in Hec1B cells expressing WT and MT miR-122, respectively, although the level of replication was lower in cells infected with HCVcc-M2 than in those infected with HCVcc, probably due to the mutations in the 5′ UTR (Fig. 8F). In contrast, a mutant virus (HCVcc-M1) bearing a mutation in site 1 alone exhibited efficient replication in Hec1B cells expressing both WT and MT miR-122 comparable to the replication level of the wild-type virus in cells expressing WT miR-122. Furthermore, the replication level of HCVcc-M1 was low in Hec1B cells expressing either WT or MT miR-122, suggesting that interaction between miR-122 and either of the seed sequence-binding sites in the 5′ UTR has an equal ability to enhance the replication of the HCV genome. However, it was shown that the